AD-A067 586 AUBURN UNIV ALA DEPT OF AEROSPACE ENGINEERING F/G 20/4
AN AERODYNAMIC ANALYSIS OF DEFORMED WINGS IN SUBSONIC AND SUPER--ETC(U)
MAR 78 J E BURKHALTER, M E VAUGHN DAAG29-78-G-0036
UNCLASSIFIED NL

1 OF 1
AD
A067586

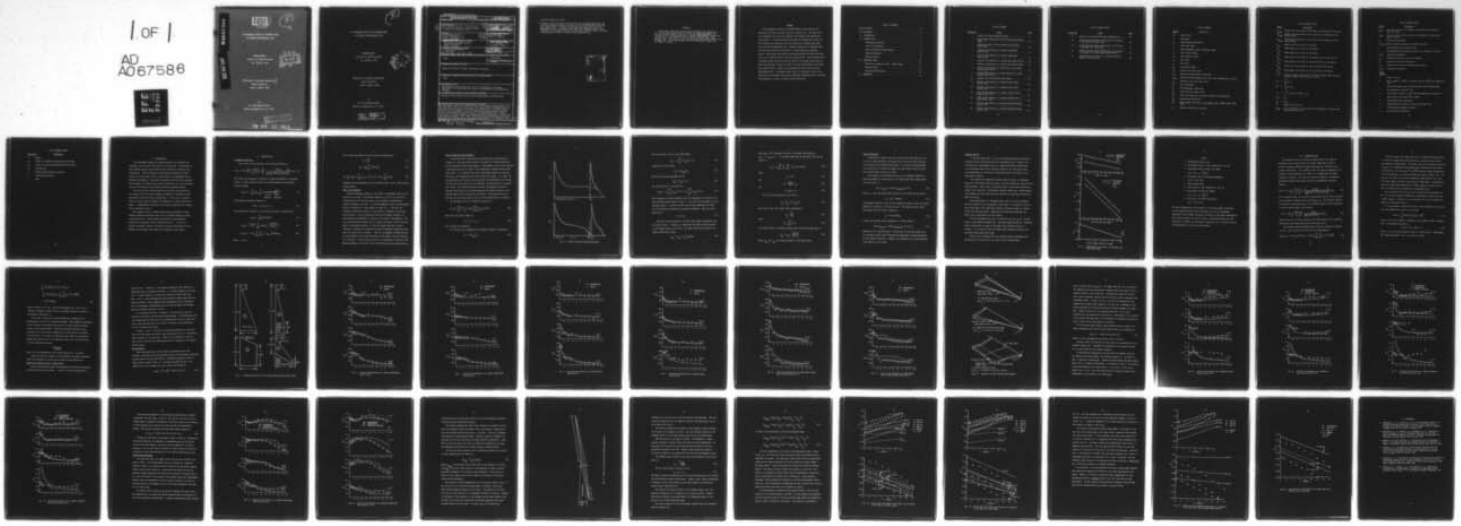

END
DATE
FILMED
6 -79
DDC

LEVEL III

A052449

5

AN AERODYNAMIC ANALYSIS OF DEFORMED WINGS IN SUBSONIC AND SUPERSONIC FLOW

INTERIM REPORT

Contract No. DAAG29-78-G-0036

Jan. 1978-Dec. 1978

Department of Aerospace Engineering

Auburn University

Auburn, Alabama 36830

for

U.S. Army Research Office

Research Triangle Park, N.C. 27709

(5)

AN AERODYNAMIC ANALYSIS OF DEFORMED WINGS IN SUBSONIC AND SUPERSONIC FLOW

INTERIM REPORT

Contract No. DAAG29-78-G-0036

Jan. 1978-Dec. 1978

Department of Aerospace Engineering

Auburn University

Auburn, Alabama 36830

for

U.S. Army Research Office

Research Triangle Park, N.C. 27709

Unclassified

SECURITY CLASSIFICATION OF THIS PAGE (When Data Entered)

REPORT DOCUMENTATION PAGE	READ INSTRUCTIONS BEFORE COMPLETING FORM
1. REPORT NUMBER	2. GOVT ACCESSION NO. 3. RECIPIENT'S CATALOG NUMBER
4. TITLE (and Subtitle) (6) An Aerodynamic Analysis of Deformed Wings in Subsonic and Supersonic Flow,	5. TYPE OF REPORT & PERIOD COVERED (9) Interim Report - Jan[illegible]-Dec[illegible]78, (12)
	6. PERFORMING ORG. REPORT NUMBER
7. AUTHOR(s) (10) John E. Burkhalter, Milton E. Vaughn, Jr. John M. Abernathy	8. CONTRACT OR GRANT NUMBER(s) (15) DAAG29-78-G-0036
9. PERFORMING ORGANIZATION NAME AND ADDRESS Engineering Experiment Station Auburn University Auburn, AL 36830	10. PROGRAM ELEMENT, PROJECT, TASK AREA & WORK UNIT NUMBERS (12) 54p.
11. CONTROLLING OFFICE NAME AND ADDRESS U. S. Army Research Office P. O. Box 12211 Research Triangle Park, NC 27709	12. REPORT DATE (11) Mar[illegible]78 13. NUMBER OF PAGES 53
14. MONITORING AGENCY NAME & ADDRESS(if different from Controlling Office) SAME	15. SECURITY CLASS. (of this report) unclassified 15a. DECLASSIFICATION/DOWNGRADING SCHEDULE

16. DISTRIBUTION STATEMENT (of this Report)

Approved for public release; distribution unlimited.

17. DISTRIBUTION STATEMENT (of the abstract entered in Block 20, if different from Report)

SAME

18. SUPPLEMENTARY NOTES

The findings in this report are not to be construed as an official Department of the Army position, unless so designated by other authorized documents.

19. KEY WORDS (Continue on reverse side if necessary and identify by block number)

Aerodynamic Wing Loading, Elevon Loading, Hinge Moments, Deformed Wings

20. ABSTRACT (Continue on reverse side if necessary and identify by block number)

The aerodynamic loading for deformed wings in both subsonic and supersonic flow has been under study for the past year. The basic solution technique falls into the potential flow category with appropriate restrictions. A lifting surface kernel function formulation is used for both subsonic and supersonic flow and results are obtained which agree very well with experimental data. Subsonic solutions for deformed wings with deflected elevons are obtained in a semi-closed form summation manner. Cases under study which include gaps between the elevon wing are as yet incomplete but is presently being pursued. For supersonic flow,

over

DD FORM 1 JAN 73 1473 EDITION OF 1 NOV 65 IS OBSOLETE

Unclassified

SECURITY CLASSIFICATION OF THIS PAGE (When Data Entered)

401 926

Block #20 (Abstract) Cont'd.

a modified Evvard solution forms the basis for the planar wing cases and vorticity paneling is added to account for local deformations in the wing mean camber surface. Results are obtained which agree very well with experimental data. The gapped elevon cases for supersonic flow is also analyzed and preliminary results have identified thickness effect, as being very important, at least for small elevon deflections.

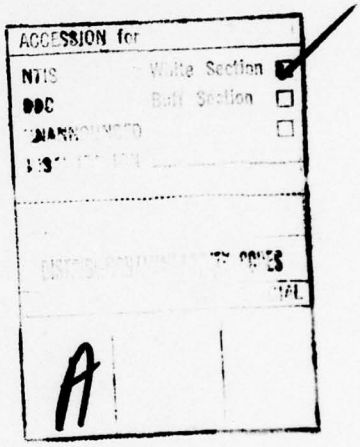

PREFACE

The work as reported in this document represents the completion of the various tasks as prescribed in Contract No. DAAG29-78-G-0036, for the Army Missile Command, Huntsville, Alabama. This research is monitored through the U.S. Army Research Office, Research Triangle Park, North Carolina, and is the result of the work done during the period January 1978-December 1978. The program manager with the Army Missile Command was Dr. Donald J. Spring.

SUMMARY

The aerodynamic loading for deformed wings in both subsonic and supersonic flow has been under study for the past year. The basic solution technique falls into the potential flow category with appropriate restrictions. A lifting surface kernel function formulation is used for both subsonic and supersonic flow and results are obtained which agree very well with experimental data. Subsonic solutions for deformed wings with deflected elevons are obtained in a semi-closed form summation manner. Cases under study which include gaps between the elevon and wing are as yet incomplete but is presently being pursued. For supersonic flow, a modified Evvard solution forms the basis for the planar wing cases and vorticity paneling is added to account for local deformations in the wing mean camber surface. Results are obtained which agree very well with experimental data. The gapped elevon cases for supersonic flow is also analyzed and preliminary results have identified thickness effect, as being very important, at least for small elevon deflections.

TABLE OF CONTENTS

LIST OF FIGURES

LIST OF FIGURES (CONT)

LIST OF SYMBOLS

Symbol	Definition
AR	Aspect ratio
b	Wing span
B_L	Wing loading coefficients
c	Local wing chord
$\bar{c}$	Mean aerodynamic chord, reference length
c_w	Local chord of wing
c_E	Local chord of elevon
c_R	Root chord
c_T	Tip chord
c_{To}	Total chord length
cc_ℓ	Section lift coefficient
cc_m	Section pitching moment coefficient
cc_{mrc}	Sectional pitching moment about root chord leading edge (y axis)
c_{ℓ_α}	Sectional lift curve slope (α=0)
C_L	Lift coefficient
C_m	Pitching moment coefficient
C_{L_α}	Total lift curve slope (α=0)
C_{L_δ}	Lift curve slope due to elevator deflection (α=0)($dC_L/d\delta$)
C_{D_i}	Induced drag coefficient
C_H	Hinge moment coefficient = $M_{HL}/(qs_E\bar{c}_E)$, M_{HL} = moment about hinge line.
C_p	Pressure coefficient, $(p-p_\infty)/q_\infty$

Symbol	Definition
$C_{N_{w(B)}}$	Normal force coefficient of the wing in the presence of the body.
$C_{N_{E(wB)}}$	Normal force coefficient of the elevon in the presence of the wing and body.
$C_{H_{E(wB)}}$	Hinge moment coefficient of the elevon in the presence of the wing and body.
$C_{N_{\alpha w}}$	Normal force curve slope of the wing.
$C_{N_{\alpha_E}}$	Normal force curve slope of the elevon.
$C_{H_{\alpha_E}}$	Hinge moment curve slope of the elevon.
$C_{N_{\delta_{E_1}}}$	Normal force curve slope of the forward strip of the elevon.
$C_{H_{\delta_{E_1}}}$	Hinge moment curve slope of the forward strip of the elevon.
$C_{N_{\delta_{E_2}}}$	Normal force curve slope of the aft strip of the elevon.
$C_{H_{\delta_{E_2}}}$	Hinge moment curve slope of the aft strip of the elevon.
ΔC_p	Pressure loading coefficient, difference between upper and lower surface pressure coefficients at a point.
$E_m = \sum_{n=0}^{N} B_L I_n$	
$F_m = \sum_{n=0}^{N} B_L I_{n+1}$	
$G_m = \int_0^{\pi/2} \sin 2\theta_o \sin (2m+1)\theta_o \, d\theta$	
$F(1) = F_{m=1}$	
$E_o = E_{m=0}$	
HL	Hinge line of elevon.
$k_{E(B)}$	Lift ratio factor of the elevon in the presence of the body with elevon deflection only.

LIST OF SYMBOLS (CONT)

Symbol	Definition
$K_{w(B)}$	Lift ratio factor of the wing in the presence of the body at angle of attack.
$K_{E(B)}$	Lift ratio factor of the elevon in the presence of the body at angle of attack.
M_∞	Freestream Mach number.
$P(x_o,y_o)$	Pressure loading parameter from Evvard solution.
S	Wing planform area, reference area
w	Non-dimensional perturbation velocity W/V_∞ parallel to z-axis.
x,y,z	Cartesian coordinates.
x_{cp}	Chordwise location of center of pressure.
x_H	Hinge line location along x-axis.
x_{LE}	Distance from y-axis to leading edge of wing.
x_o,y_o	Integration variables.

Greek Symbols

α	Angle of attack.
β	Mach parameter, $\sqrt{1-M_\infty^2}$ for subsonic flow and $\sqrt{M_\infty^2-1}$ for supersonic flow.
ε	Gap width between wing trailing edge and elevon leading edge.
γ	Non-dimensional vorticity Γ/V_∞.
δ	Elevon angle relative to wing (trailing edge down is positive).
λ	Taper ratio, (tip chord)/(root chord).
Λ	Wing leading edge sweep angle.
ϕ	Nondimensional perturbation velocity potential ϕ/V_∞.
θ	Non-dimensional spanwise variable.
ξ,η	Non-dimensional variables.

Subscripts	Definition
E	Elevon
nm	Points or constants associated with the wing.
pq	Points or constants associated with the elevon.
LE	Leading edge
o	Denotes wing coordinate variables
∞	Freestream conditions.
w	Wing.

I. INTRODUCTION

The aerodynamic loading for deformed wings in both subsonic and supersonic flow has been under study for the past year. The problem of wing loading solutions have generally been confined to potential flow formulations. These solutions have been applied primarily to planar wings but in some cases, such as vortex lattice, are applicable to the deformed wing problem. The present formulation falls into the potential flow category, but unlike vortex lattice techniques, is of the continuous vorticity distribution type yielding continuous loading profiles.

Not only are local wing deformations included in the analysis but for subsonic flow, the elevon loading is computed for displaced elevons (gap between elevon and wing trailing edge). In all cases, sectional as well as total loads and moments are computed in a "semi" closed form manner. A comprehensive discussion of the basic formulation for subsonic flow is presented in Ref. 1.

For supersonic flow, a similar kernel function approach is taken leading to general functional forms for the localized loading on wings in supersonic flow. A more complete derivation of the applicable equations for supersonic flow is presented in Ref. 1. In order to preserve continuity, however, the general equations applicable for both subsonic and supersonic flow regimes are repeated in this report.

II. SUBSONIC FLOW

Fundamental Equations

For a planar lifting surface, the potential equation is

$$\phi(x,y,z) = \frac{1}{4\pi} \iint_S \frac{\gamma(x_o,y_o)}{(y-y_o)^2+z^2} z \left(1 + \frac{(x-x_o)}{\sqrt{(x-x_o)^2+\beta^2(y-y_o)^2+\beta^2 z^2}}\right) dx_o\, dy_o \quad (1)$$

The closed form integration technique for wing sub-elements as described in Ref. 1 yields excellent results for planar wings with the assumed pressure loading

$$\Delta C_p(\xi,\eta) = \sum_{n=0}^{N} \frac{1}{c(\eta)} \sum_{m=0}^{M} B_L \underbrace{\sin(2m+1)\theta}_{\text{Spanwise}} \underbrace{\sqrt{\frac{1-\xi}{\xi}}\, \xi^n}_{\text{Chordwise}} \quad (2)$$

The applicable boundary condition is

$$w(x,y) + \sin \alpha(x,y) = 0 \quad (3)$$

and solutions are obtained for the various sectional coefficients as

$$cc_\ell(y_o) = \sum_{m=0}^{M} E_m \sin(2m+1)\theta \ . \quad (4)$$

$$cc_d(y_o) = \frac{cc_\ell(y_o)}{8} \sum_{m=0}^{M} (2m+1) E_m \frac{\sin(2m+1)\theta_o}{\sin \theta_o} \quad (5)$$

$$cc_m(y_o) = -c(y_o) \sum_{m=0}^{M} \sum_{n=0}^{N} B_L \ I_{n+1} \sin(2m+1)\theta_o \quad (6)$$

where $L = Nm + n$.

Total forces and moments are then found by integration as

$$C_L = \frac{\pi E_o}{2S} \tag{7}$$

$$C_{D_i} = \frac{\pi}{16S} \sum_{m=0}^{M} (2m+1) E_m^2 \tag{8}$$

$$C_m = \frac{1}{S\bar{c}} \left[(c_R - c_T) \sum_{m=0}^{M} F_m G_m - \frac{\pi}{2} c_R F(1) - \tan \Lambda \sum_{m=0}^{M} E_m G_m \right] \tag{9}$$

Comparison with experimental data is excellent (Ref. 1) for a wide variety of wing shapes.

Order of Polynomials

Before proceeding, comments on the effect of polynomial order on the solution is in order. The unknown constants, B_L in Eq. (2) are really coefficients for the various terms in the polynomial describing the pressure loading on the wing. It has been suggested that if the polynomial order is increased to a large number of terms (i.e., > 50) that the sectional coefficients such as cc_ℓ will tend to "oscillate" in the spanwise direction. For the formulation used in the present analysis, no oscillations are observable at least up to 50 terms in the equation. However, oscillations do indeed occur if terms on the order of 80 or more are used in the pressure loading. It does not appear that this is due to "numerical" instability as would be the case if numerical integration were used, but rather due to overkill. That is, the pressure loading function is rather general and for most wings only a few terms (< 20) are required for a solution. If more terms are used, it is analogous to fitting a 50th degree polynomial to a linear curve; oscillations are the inevitable results.

Elevon Loading and Hinge Moments

For the past year, concentration has been placed on predicting the loading of a full span elevon placed in the wake of a lifting surface and on the associated elevon hinge moments. Displacement of the elevon creating a wing-elevon gap and its effect on the wing-elevon loading has also been under study. It is apparent that when a gap exists between the wing and the elevon, the loading distributions on each will change. For a gap, the wing and elevon are treated as two wings with the requirement that the gap is less than local wing chord, and therefore, the wing wake has no significant rollup. Two loading functions are used, satisfying the infinite pressure differential at the leading edge and the Kutta condition at the trailing edge of both the wing and the elevon. The assumed loading for both the gap and the gap-sealed cases are shown schematically in Figure 1.

The sectional lift for a wing with an elevon is

$$cc_{\ell}(y_o) = \int_{x=0}^{x=c_w} \Delta C_{p_w}(\xi,\eta)dx + \int_{x=(c_w+\varepsilon)}^{x=c_{T_o}} \Delta C_{p_E}(\xi,\eta)dx \tag{10}$$

where the total chord length is

$$c_{T_o} = c_w + c_E + \varepsilon \tag{11}$$

and ε denotes the gap width.

For the wing, the nondimensional chordwise variable is defined as

$$\xi_w = (x-x_{LE_w})/c_w \tag{12}$$

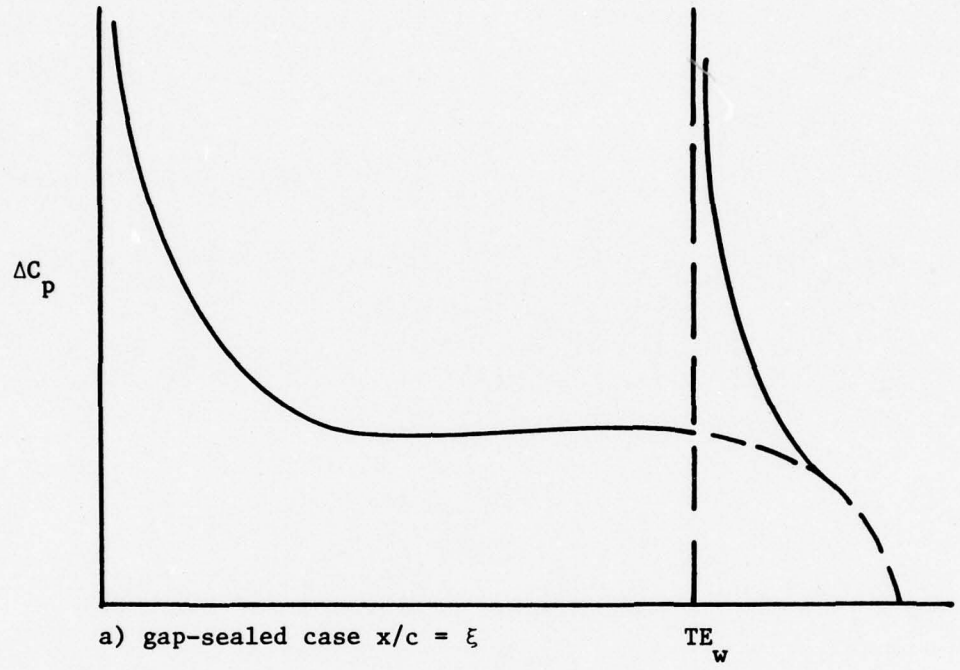

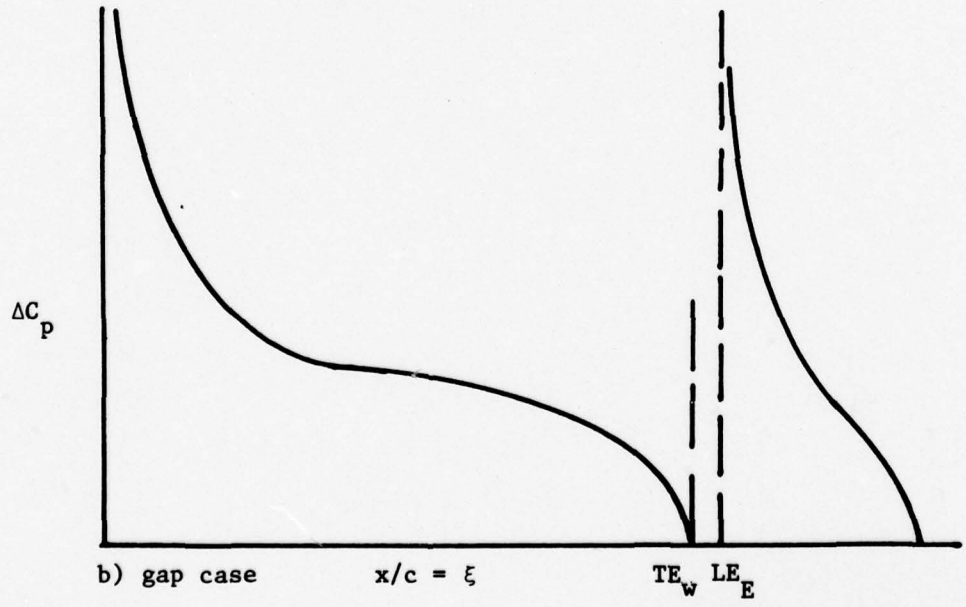

Fig. 1. Typical Chordwise Loading Functions.

and the sectional lift for the wing becomes

$$cc_{\ell_w} = c_w \int_{\xi=0}^{\xi=1} \Delta C_{p_w}(\xi_w,\eta)\, d\xi \tag{13}$$

Similarly, for the elevon,

$$\xi_E = (x-x_{LE_E})/c_E \tag{14}$$

where the elevon leading edge is now

$$x_{LE_E} = x_{LE_w} + c_w + \varepsilon \tag{15}$$

The sectional lift is now given by

$$cc_\ell(y_o) = c_w \int_{\xi_w=0}^{\xi_w=1} \Delta C_{p_w}(\xi,\eta)\, d\xi + c_E \int_{\xi_E=0}^{\xi_E=1} \Delta C_{p_E}(\xi,\eta)\, d\xi \tag{16}$$

Each integral is treated separately and the integration is carried out as with the wing alone analysis of Ref. 1. The total lift and moment is also similarly found. It should be noted that the gap dimensions are small and are excluded in defining all reference dimensions. Thus the total wing area is

$$S = S_w + S_E \tag{17}$$

Extension of this analysis to include hinge moment computations was also done in Ref. 1. However, by definition the hinge line was located at the leading edge of the elevon. For other hinge line locations, the moment coefficient becomes

$$c_{m_{HL}} = c_{m_{LE}} + c_{L_E}\,(x_{HL}/\bar{c}_E) \tag{18}$$

where x_{HL} is the chordwise location of the hinge line defined by $x_{HL} = x - x_{LE_w} - c_w - \varepsilon$. It has been shown that the sectional lift for the elevon is

$$cc_{\ell_E} = c_E \sum_{p=0}^{N_E} \frac{1}{c_E} \sum_{q=0}^{M_E} I_p B_L \sin (2q+1)\theta \tag{19}$$

where

$$I_o = \pi/2 \tag{20}$$

and

$$I_p = \left(\frac{2p-1}{2p+2}\right) I_{p-1} \tag{21}$$

and

$$L = (N_E)\, q + p. \tag{22}$$

The total lift produced by the elevon is

$$C_{L_E} = \frac{2}{S_E} \int_0^1 cc_{\ell_E}(\eta)\, d\eta \tag{23}$$

Using (19) in Eq. (23) yields (after integration)

$$C_{L_E} = \frac{\pi H_o}{2S_E} \tag{24}$$

where

$$H_q = \sum_{p=0}^{N_E} B_L I_p \tag{24}$$

In a similar manner the moment produced about the elevon hinge line is

$$C_{m_{HL}} = C_{m_{LE}} + \frac{\pi H_o}{2S_E} \frac{x_{HL}}{\bar{c}_E} \tag{25}$$

where $C_{m_{HL}}$ and $C_{m_{LE}}$ are moments produced by the elevon only.

Wing Deformations

A wing which is warped such that all points on the wing do not lie in the x-y plane presents a different view to the flow field from that of the planar wing considered previously. To account for wing warpage, it is necessary to consider the angle that each control point and each grid element makes with the x-y plane.

For warpage in the chordwise direction, the downwash produced by each grid element is proportional to the angle which that element makes with the x-axis, or

$$\Delta w(x,y)_{warped} = [\Delta w(x,y)_{unwarped}] \cos \alpha_i \tag{26}$$

where α_i is the wing slope angle relative to the x-axis and is given by

$$\alpha_i = \tan^{-1} (dz/dx)_i \tag{27}$$

The boundary condition is for no flow through the wing, or that the normal component of velocity to the wing be zero. The angle that the control point makes with the x-axis is given by

$$\alpha_c = \tan^{-1}(dz/dx)_c \tag{28}$$

so that the downwash from a sublement at a control point is

$$\Delta w(x,y)_{warped} = [\Delta w(x,y)_{unwarped}] \cos (\alpha_i - \alpha_c) \tag{29}$$

Definition of a wing deformation function z(x) of the mean camber line can therefore produce many variations and amplitudes of wing distortions in the chordwise direction. However, the condition of no flow separation still applies at all points.

Subsonic Results

It has been shown (Ref. 1) that the preceeding wing-elevon analysis produces results which agree well with experimental data. However, the availability of experimental data for a gapped wing-elevon combination, or for deformed wings is very limited; therefore, for the present time, the investigation is restricted to predicting results and trends of the theoretical analysis.

The research was conducted using two types of wings, a rectangular wing, and a low aspect ratio delta wing. Four variations were used for each wing planform; a planar chord, a wing with twist, a wing with circular arc camber, and a wing with a sinusoidally deformed camber line. Hinge moments, total moment, and total lift were then computed for varying gap sizes and angles-of-attack.

The computations for the gapped elevon cases are as yet incomplete and will therefore not be presented in this report. At present, it may be stated that gaps at the wing-elevon juncture certainly change the loading on both the wing and elevon. Quantitative calculations regarding this effect will be presented in a later report.

For the non-gapped case, Fig. 2 illustrates C_{H_α} and C_{H_δ} for a planar versus a sinusoidally deformed wing. The hinge moment slopes for a deformed wing is essentially the same as the planar wing, differing only by a constant. It is seen also that the hinge moment decreased linearly with increased leading edge camber angle.

Several other configurations are currently being investigated with varying types of deformations as listed in the following table.

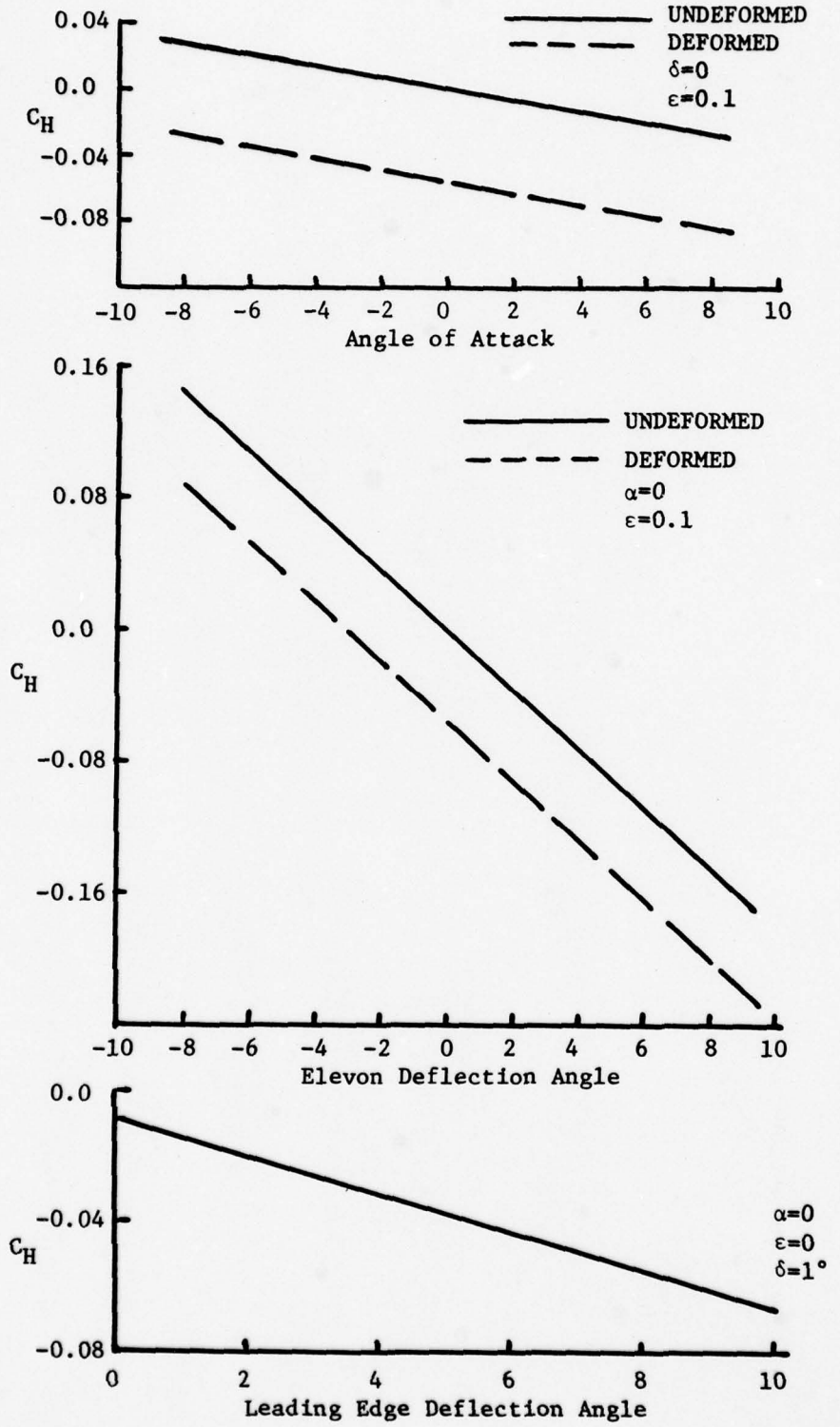

Fig. 2. Hinge Moment Coefficient for Deformed and Undeformed Wings.

TABLE

1. Rectangular, planar wing.
2. Rectangular wing, 6° twist (washout) at the tip.
3. Rectangular wing, circular arc camber

   $z(x) = [r^2 - (x - \frac{C_w}{2})^2]^{\frac{1}{2}}$

4. Rectangular wing, sinusoidal deformation

   $z(x) = A \sin (2\pi x)$

5. Delta, planar wing
6. Delta wing, 6° twist (washout) at the tip
7. Delta wing, circular arc camber

   $z(x) = [r^2 - (x - \frac{C_w}{2})^2]^{\frac{1}{2}}$

8. Delta wing, sinusoidal deformation

   $z(x) = A \sin (2\pi x)$

For each configuration, the dependence of the hinge moment coefficient on the hingeline location and on the gap size is to be determined. Dependence on Mach number and angle of attack is still under investigation with results expected in the near future. Definitive efforts are also under way to quantify the dependence of gap size, etc., on total lift and pitching moment of the entire configuration.

III. SUPERSONIC FLOW

The analysis used in the present research effort for wings in supersonic flow is based in part on Evvards theory and in part on vorticity paneling leading to simple expressions for the basic aerodynamic coefficients. As in subsonic flow, the wing is subdivided into a number of small subpanels over which it is assumed that the panel strength is constant. The vorticity panel is actually a continuously distributed doublet panel which satisfies the supersonic potential equation

$$\phi(x,y,z) = \frac{1}{2\pi} \iint_{S_o} \frac{\gamma(x_o,y_o)}{(y-y_o)^2+z^2} z \left(\frac{(x-x_o)}{\sqrt{(x-x_o)^2-\beta^2(y-y_o)^2-\beta^2z^2}} \right) dx_o dy_o \tag{30}$$

As for subsonic flow, the vorticity distribution $\gamma(x_o,y_o)$ may be replaced by the pressure loading coefficient $\frac{1}{2}\Delta C_p(x_o,y_o)$. The downwash equation is obtained by differentiation in the standard manner and when evaluated in the z=0 plane (planar flow) becomes

$$w(x,y) = \frac{1}{4\pi} \iint_{S_o} \frac{\Delta C_p(x_o,y_o)}{(y-y_o)^2} \frac{(x-x_o)}{\sqrt{(x-x_o)^2-\beta^2(y-y_o)^2}} dx_o dy_o \tag{31}$$

where the area S_o is that contained on the wing surface in the upstream running Mach cone emanating from the field point (x,y).

The assumed pressure loading differs from that previously reported in Ref. 1 and is written as the sum of two expressions as

$$\Delta C_p(x_o,y_o) = P(x_o,y_o)\sin(\alpha+\theta_o) + P(x_o,y_o) \sum_{n=0}^{N} \sum_{m=0}^{M} B_L \eta^m \cos \frac{n\pi\xi}{2} \tag{32}$$

The first term on the right-hand side is a modified Evvard solution to account for local wing deformations and is valid for both subsonic and supersonic leading edges. The second term uses the pressure functions $P(x_o,y_o)^1$ as a weighting function which, when multiplied by the unknown coefficient B_L, and the series $\eta^m \cos \frac{n\pi\xi}{2}$ accounts for small deformations in the wing surface in the upstream Mach cone from the point (x,y). The order of the terms in the second expression seldom exceeds 3 or 4 and for planar wings, the entire second term is unnecessary. Increasing the order for larger wing deformations or higher angles of attack does not seem to provide better agreement with experimental data.

As in subsonic flow, the ΔC_p term is removed from the integral in Eq. (31) and the resultant expression is integrated in closed form over a small subpanel. Results of this integration over various shaped subelements is presented in Ref. 1.

It is convenient to define the value of this integral as $\beta\Delta K$ so that the total downwash at a point (x,y) becomes

$$w(x,y) = \sum_{i=1}^{I} (\Delta K)_i [\Delta C_p(\bar{x}_o,\bar{y}_o)]_i \left(\frac{\beta}{4\pi}\right) \tag{33}$$

where I is the total number of subpanels in the region (cone) of integration. The boundary condition is

$$w(x,y) + \sin(\alpha+\theta_c) = 0 \tag{34}$$

where θ_c is the local deformation angle at a control point. Rearranging and combining Equations (32), (33) and (34) yields

$$\sum_{i=1}^{I} (\Delta K)_i [P(\bar{x}_o, \bar{y}_o) \sin(\alpha+\theta_o)]_i +$$

$$\sum_{i=1}^{I} (\Delta K)_i [P(\bar{x}_o, \bar{y}_o) \sum_{n=0}^{N} \sum_{m=0}^{M} B_L \eta^m \cos \frac{n\pi\xi}{2}]_i$$

$$= - \frac{4\pi}{\beta} \sin(\alpha+\theta_c) \qquad (35)$$

where as before L = n + mN. The above expression, Eq. (35), is conveniently arranged in matrix form for a Gaussian reduction solution of the unknown coefficient, B_L.

Body volume effects on the wing loading are accounted for by assuming that the body is cylindrically shaped. The cylinder is generated with an infinite line doublet whose axis is in the z-direction perpendicular to the wing planform. (Lifting interference effects are not accounted for in the present analysis but is under study for inclusion in future work.) The result of adding the body volume to the analysis simply adds another term to the right-hand side of Eq. (35) which after a little manipulation becomes

$$- \frac{4\pi a^2 \sin \alpha}{\beta(a+\eta)^2}$$

where a is the nondimensional body radius defined by $a = r_b/(b/2)$.

Unlike the subsonic analysis, the (supersonic) sectional properties cannot be integrated in closed form but must be done numerically.

Results for Supersonic Flow - Planar Wings

Several wing planform shapes were analyzed for which both undeformed and deformed data were available. A sketch of the four planforms are

shown in Fig. 3. Results of the pressure loading on these wings in an undeformed state are presented in Figs. 4-9 for Mach numbers of 1.61 and 2.01. In these figures, the theoretical solution is that taken from Refs. 2 and 3. Minor improvements could possibly be made using vorticity paneling; however, since agreement with experimental data is excellent, this is unnecessary. Experimental data for both the planar and deformed wings are obtained from Refs. 4 and 5.

It is apparent from Figs. 4 through 9 that the linear theory is excellent for subsonic and supersonic leading edges. The disagreement near the leading edge and wing tip is to be expected and is due to wing thickness, shocks and wing twist; the latter, of course, is not significant for the low aspect ratio wings.

In Figs. 8 and 9, the error is attributed primarily to wing twist where the wings under wind tunnel tests experienced up to 1.5° aeroelastic twist (washout) at the wing tips. Washout in the vacinity of the tip would tend to lower the ΔC_p distribution which is indicated in the experimental results.

Deformed Wings

These same wings under various kinds of deformation were also analyzed by including vorticity paneling as well as the previous theoretical loading terms in the ΔC_p distribution. Deformation shapes of three of these wings are shown in Fig. 10. The delta wing (#1) in Fig. 3 was cambered with a mean camber line curve fitted and defined by

$$(z/c_R) = \tan 3°[\tfrac{1}{4} - (\eta+\xi(1-\eta)-.5)^2] \qquad (36)$$

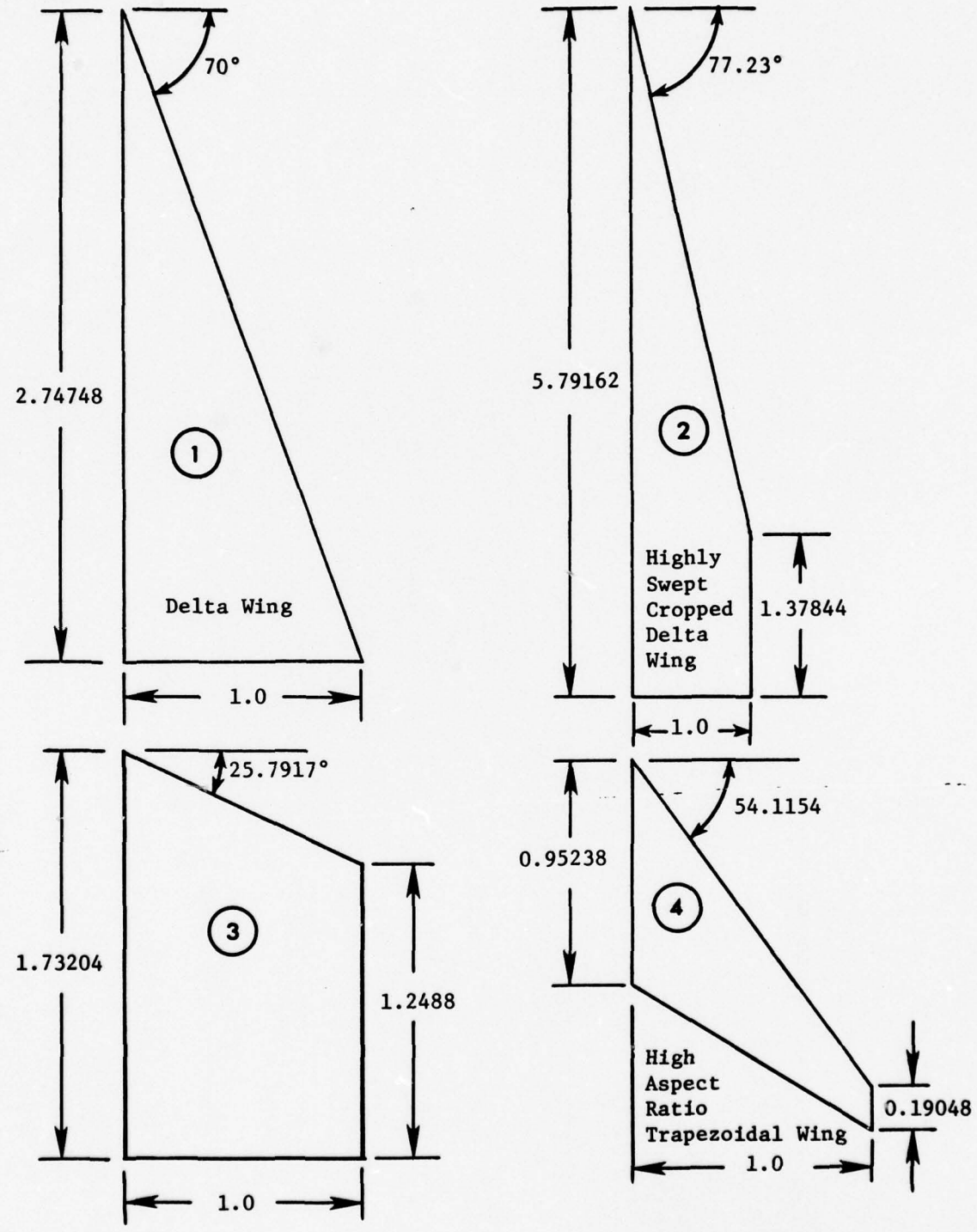

Fig. 3. Dimensional Sketch of Four Wing Planform Shapes Under Study.

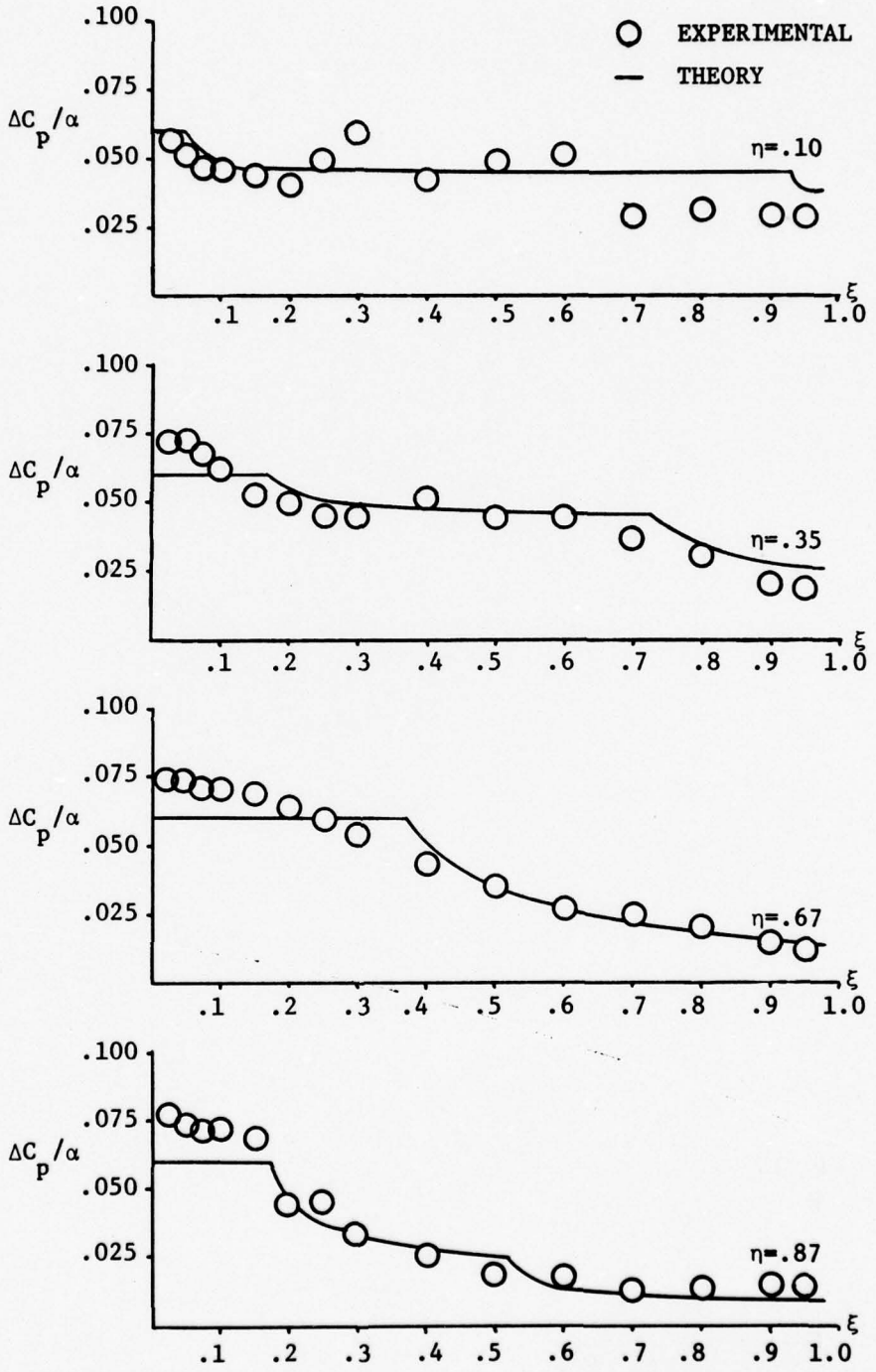

Fig. 4. Pressure Distribution on a Planar Trapezoidal Wing, M=1.61.

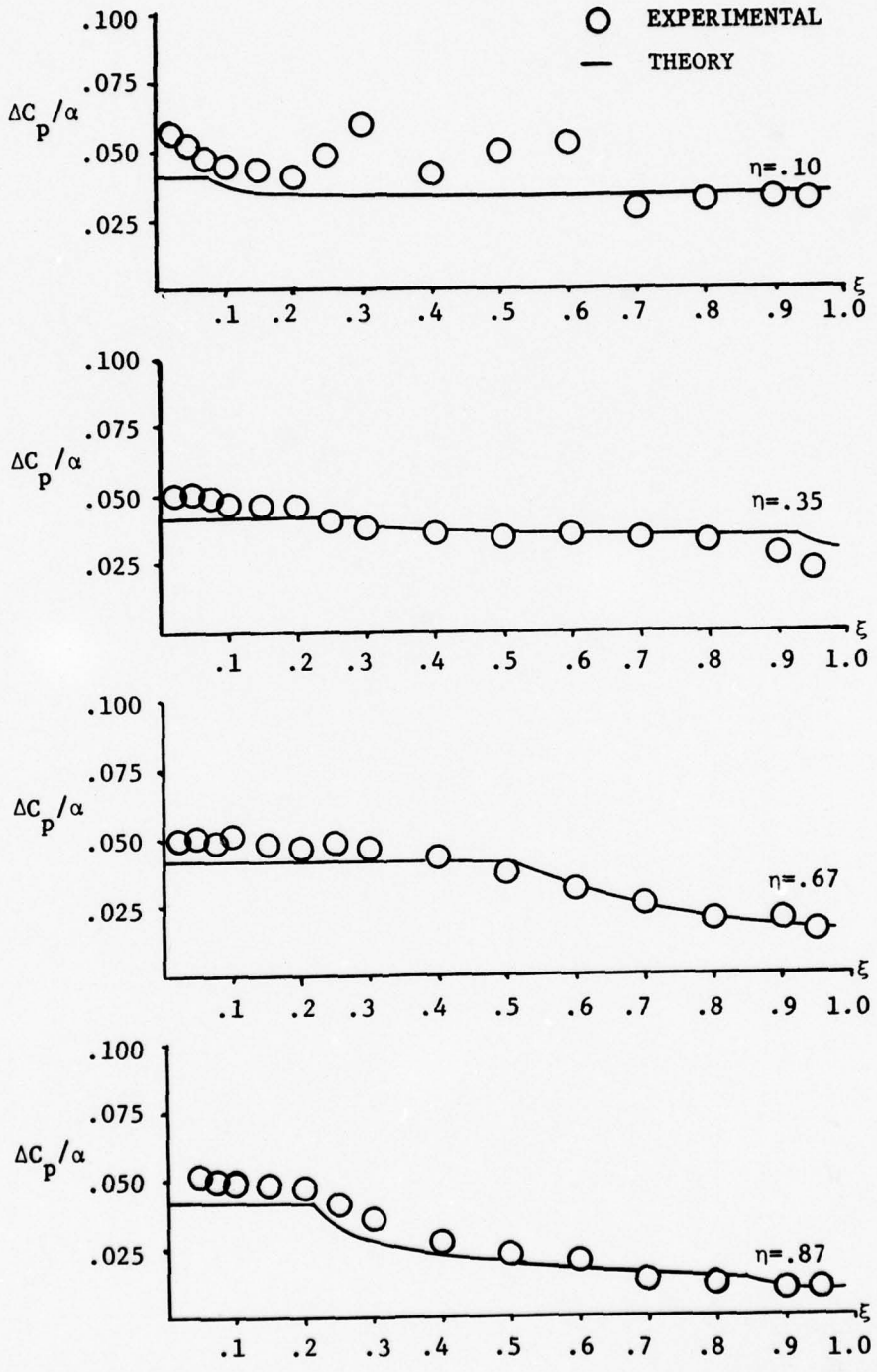

Fig. 5. Pressure Distribution on a Planar Trapezoidal Wing, M=2.01.

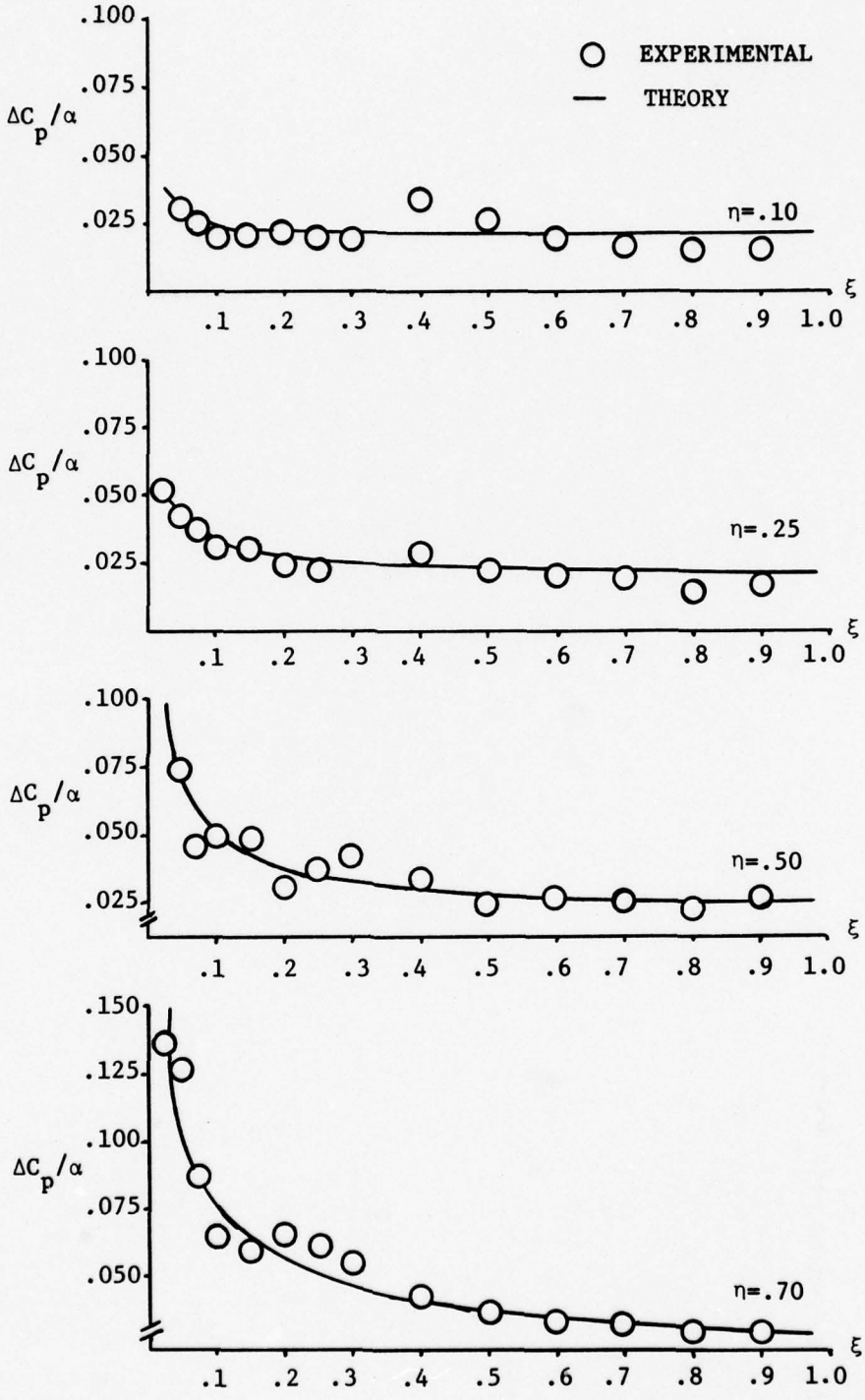

Fig. 6. Pressure Distribution on a Planar Delta Wing, M=1.61.

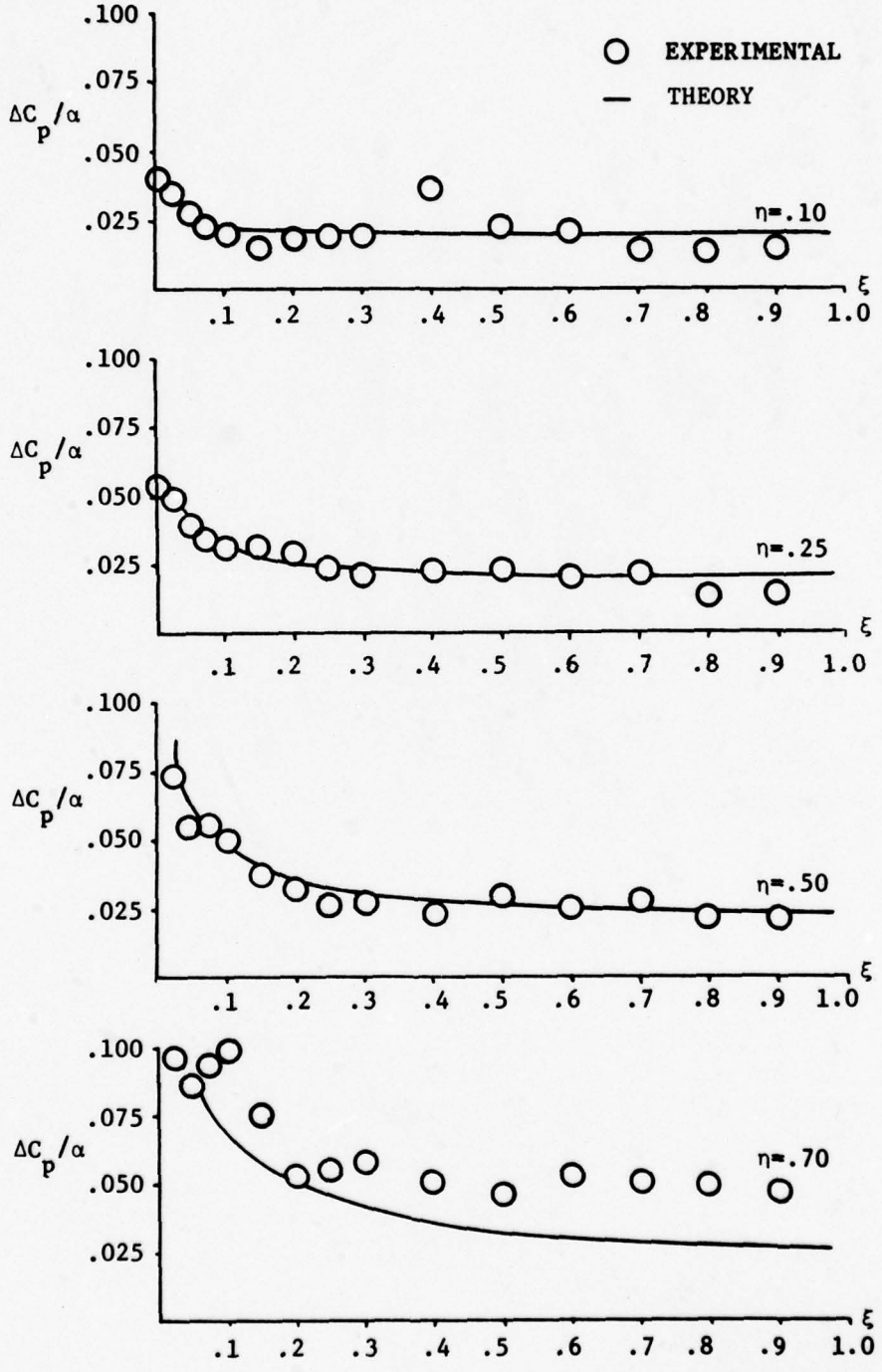

Fig. 7. Pressure Distribution on a Planar Delta Wing, M=2.01.

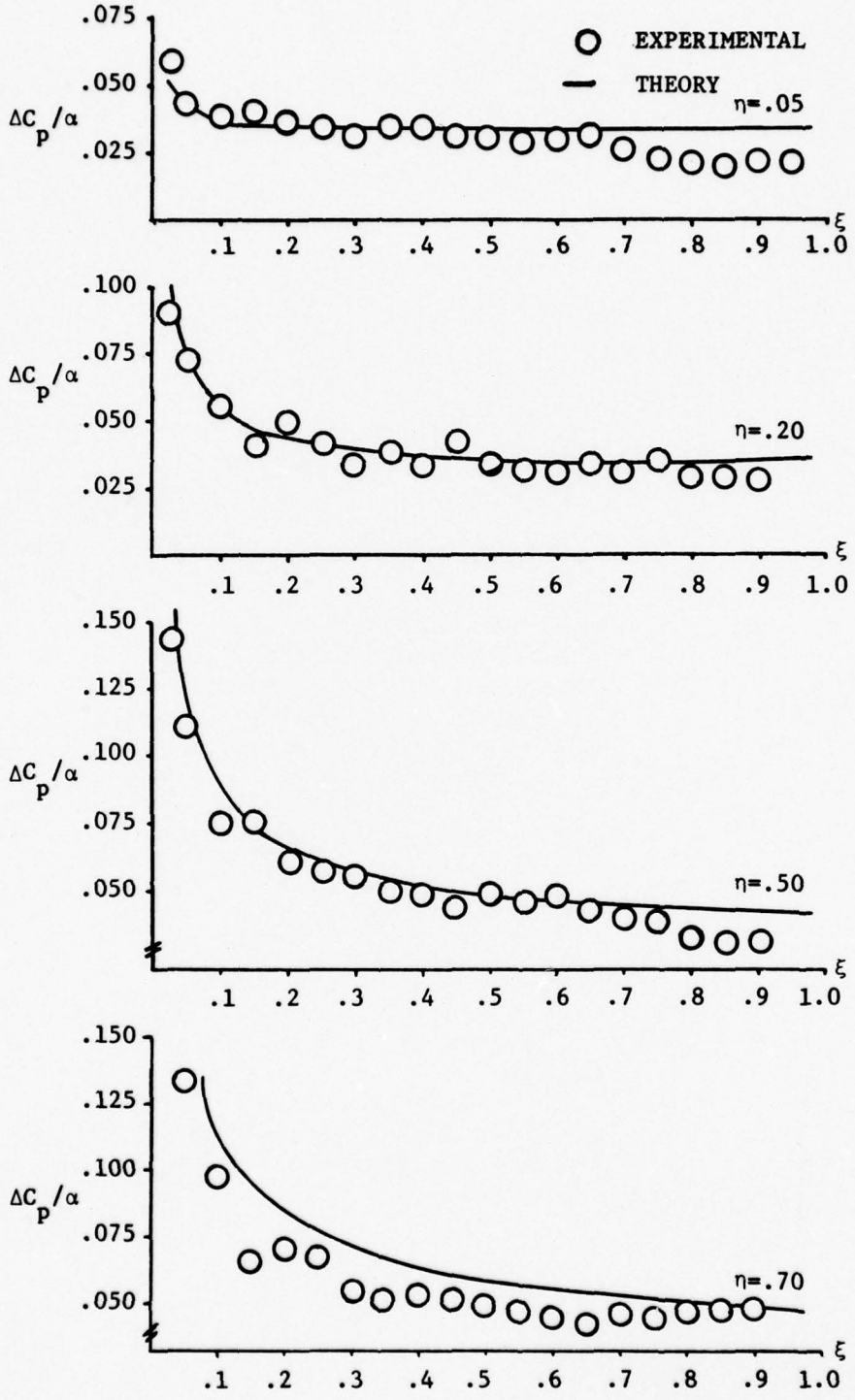

Fig. 8. Pressure Distribution on a High Aspect Ratio, Swept Tapered Wing, M=1.61.

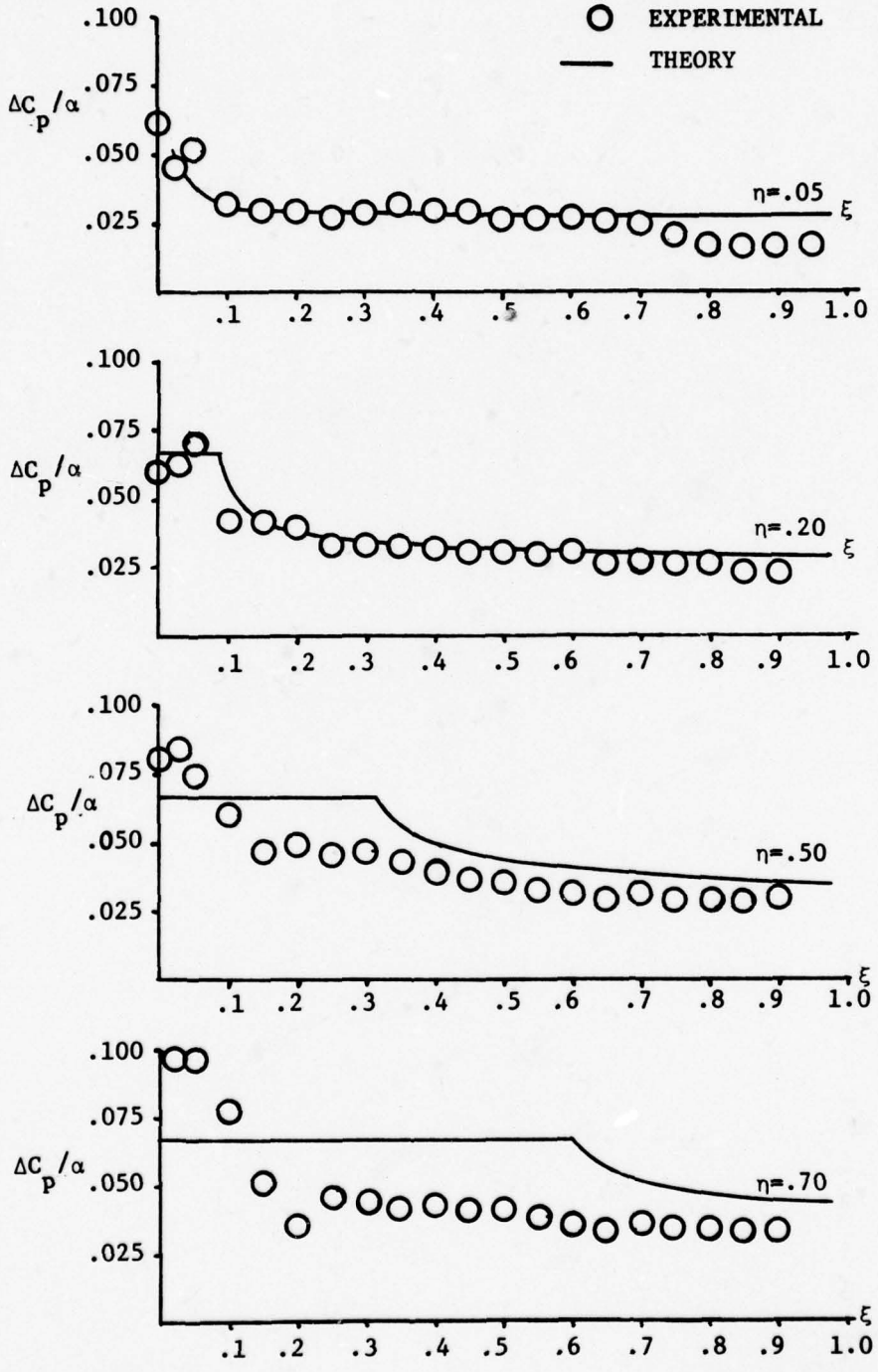

Fig. 9. Pressure Distribution on a High Aspect Ratio, Swept Tapered Wing, M=2.01.

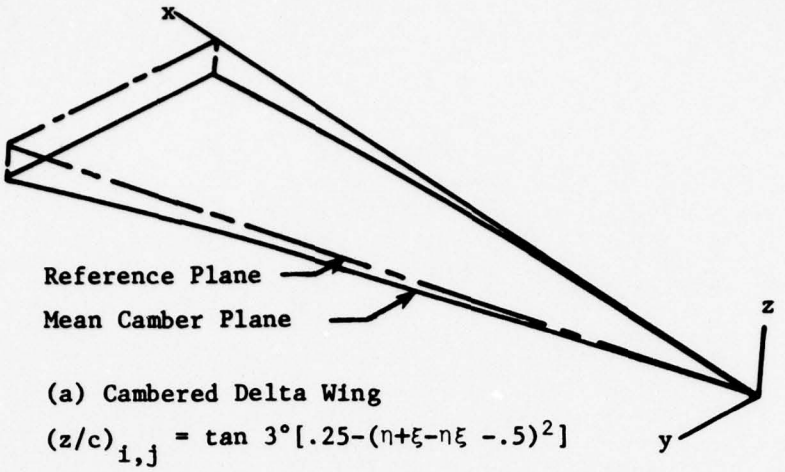

(a) Cambered Delta Wing

$(z/c)_{i,j} = \tan 3°[.25-(\eta+\xi-\eta\xi-.5)^2]$

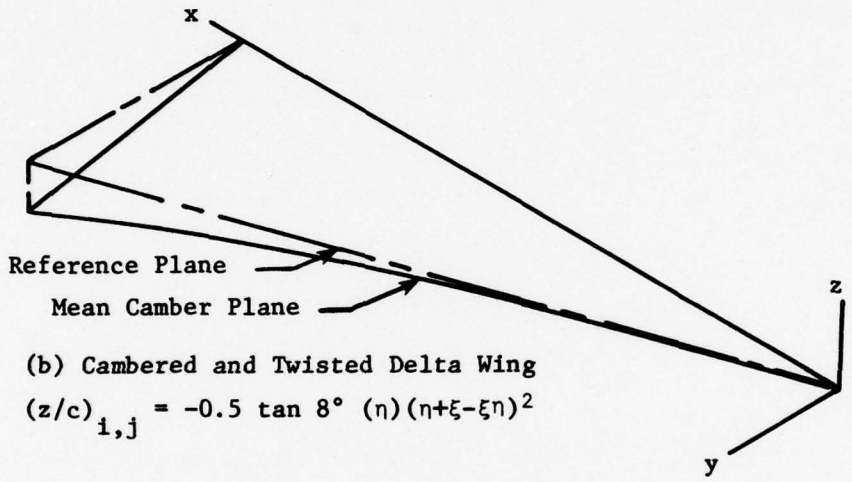

(b) Cambered and Twisted Delta Wing

$(z/c)_{i,j} = -0.5 \tan 8° \ (\eta)(\eta+\xi-\xi\eta)^2$

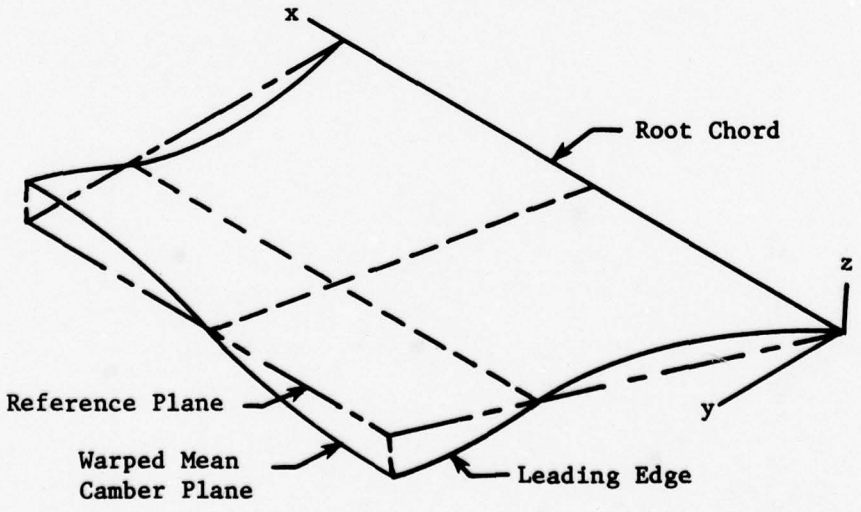

(c) Warped Trapezoidal Wing

$(z/c)_{i,j} = 0.033454 \sin (3\pi\eta/2)_i \cos(\pi\xi)_j$

Fig. 10. Schematic of Three Deformed Wing Shapes.

where $\eta=y/(b/2)$ and $\xi=(x-x_{LE})/c$. The camber (See Fig. 10) is uniform in the spanwise direction and produces a maximum deflection angle of three degrees relative to the chord line. Although this seems like a small task, this is actually a severe test of the theory and its agreement with experimental data. In Figs. 11 and 12, results are presented for the cambered delta wing at Mach numbers of 1.61 and 2.01. Agreement at the inboard stations are relatively good while outboard agreement is rather poor. However, note that in the regions where most of the wing loading occurs, the agreement is satisfactory. Additionally, the inclusion of the doublet paneling terms in the mathematical formulation provides the correct trends and an added degree of accuracy.

For the same planform shape, linear spanwise twist is added to the camber deformation such that the mean camber surface is now defined as

$$(z/c_R) = - .5(\tan 8°)(\eta)(\eta+\xi(1-\eta))^2 \qquad (37)$$

Results of this configuration are shown in Figs. 13 and 14.

Similar results are obtained for these cases as was observed for the cambered (alone) case. Agreement is acceptable at the inboard stations but is questionable at the outboard stations.

In observing the experimental data for both the cambered alone and the cambered and twisted wings, the outboard stations ($\eta > .5$) appear to have a supersonic leading edge. Whereas the high leading edge sweep angle gives rise to a subsonic leading edge. In addition, at the $\eta = 0.5$ station, a weak shock appears to be located near $\xi = .4$ for $M = 1.61$ but is not present for $M = 2.01$. Since the theory does not account for shocks, the disagreement in this region is not surprising.

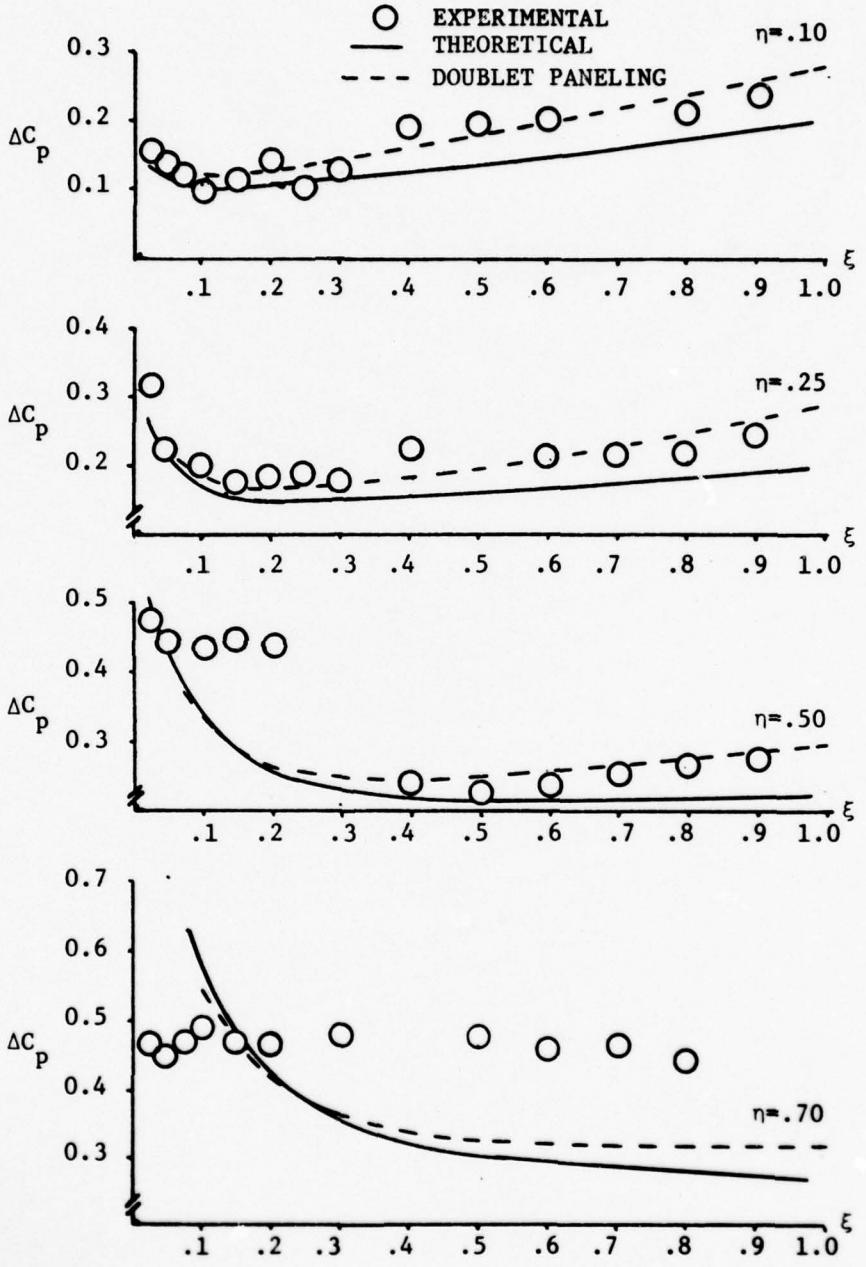

Fig. 11. Pressure Distribution on a Cambered Delta Wing, M=1.61, α=6°.

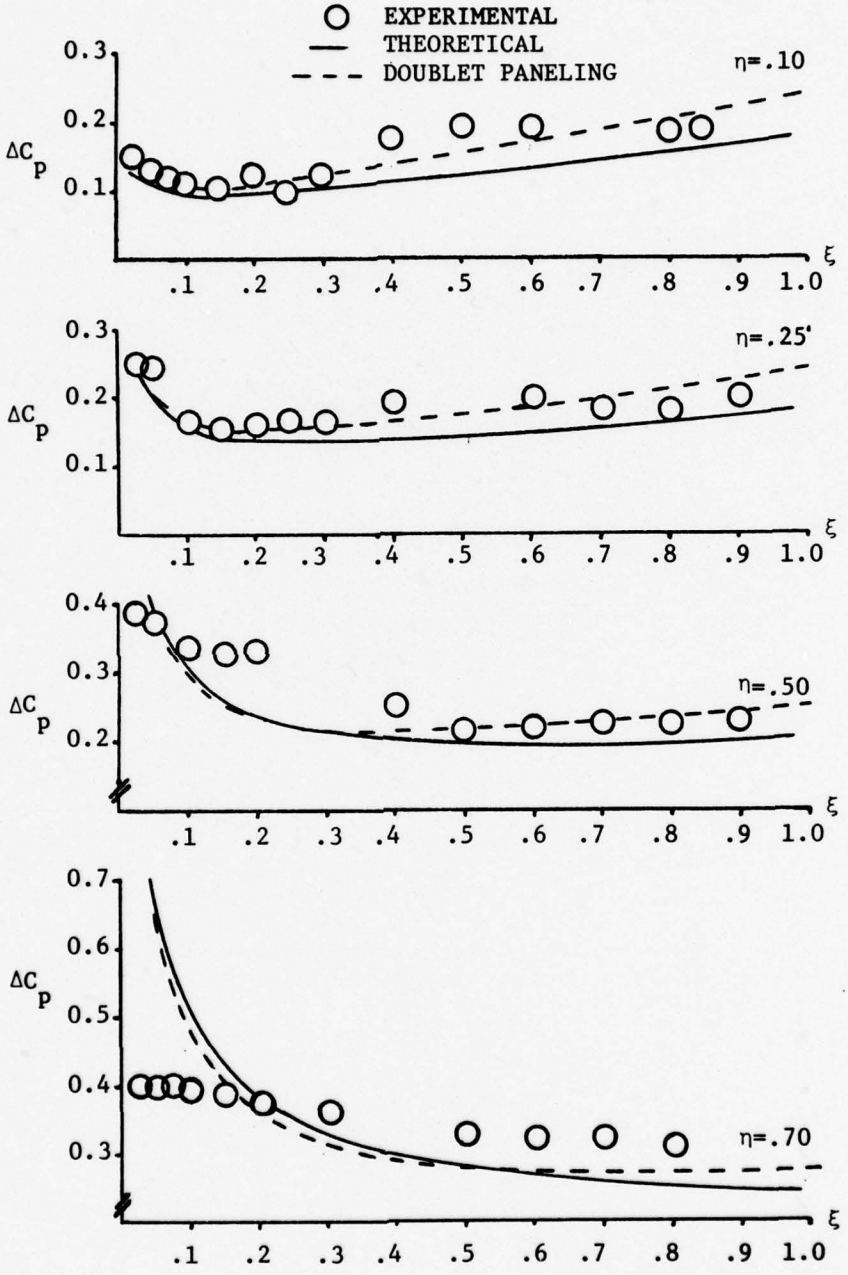

Fig. 12. Pressure Distribution on a Cambered Delta Wing, M=2.01, α=6°.

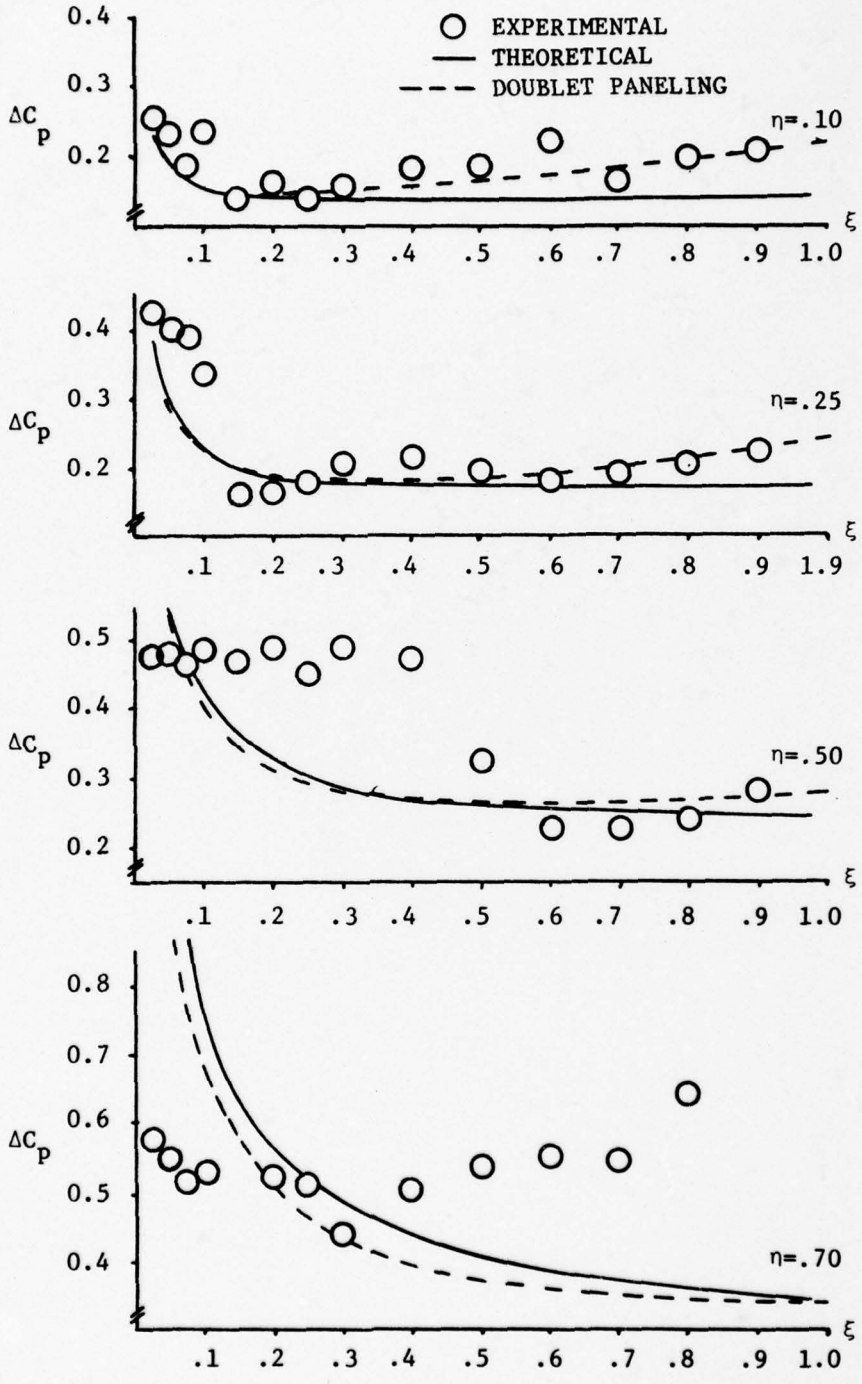

Fig. 13. Pressure Distribution on a Twisted Cambered Delta Wing, M=1.61, α=6°.

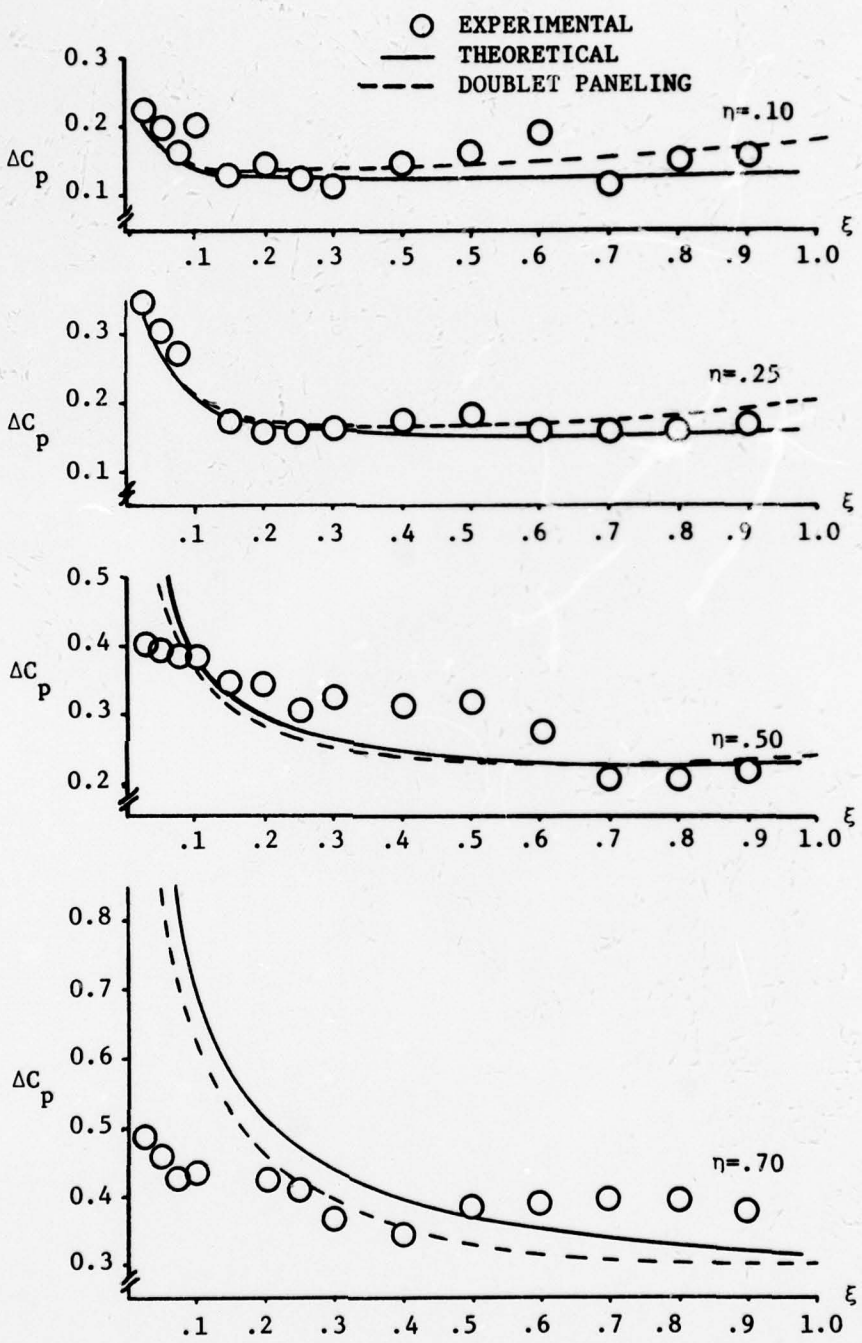

Fig. 14. Pressure Distribution on a Twisted Cambered Delta Wing, M=2.01, α=6°.

The next wing subjected to the theoretical analysis was a "warped" trapezoidal wing (See figs. 3 and 10). For both M = 1.61 and 2.01, the leading edge is supersonic and multiple "fold over" regions occur because of the low aspect ratio and the fact that the wing is trapezoidally shaped. The equation governing the mean warped camber surface is

$$(z/c)_{ij} = .033454 \sin (3\pi\eta/2)_i \cos (\pi\xi)_j \qquad (38)$$

Results for this wing are presented in Figs. 15 and 16. Considering the wing deformation, the agreement is remarkably good over the entire wing for both Mach numbers. Note also that the addition of vorticity paneling to the ΔC_p distribution predicts the right trends and correctly accounts for local wing deformations in the upstream running Mach cones.

Gapped Elevon-Thickness

For supersonic flow, the gapped elevon case was also studied in the present effort. Little experimental data is available for comparison purposes; however, one previous effort[6] did study this particular problem using a vortex lattice approach. Conclusions were drawn that the disagreement between experiment and theory was attributed to viscous effects. It is the contention of the authors of the present report that disagreement between theory and experiment is due not only to viscosity, but also to thickness effects and blockage of part of the elevon immersed in the wake of the "thick" wing.

To validate this contention, the missile configuration used in Ref. 6 was analyzed with the present theoretical approach which was modified for the thick wing-elevon configuration. A general configuration which includes

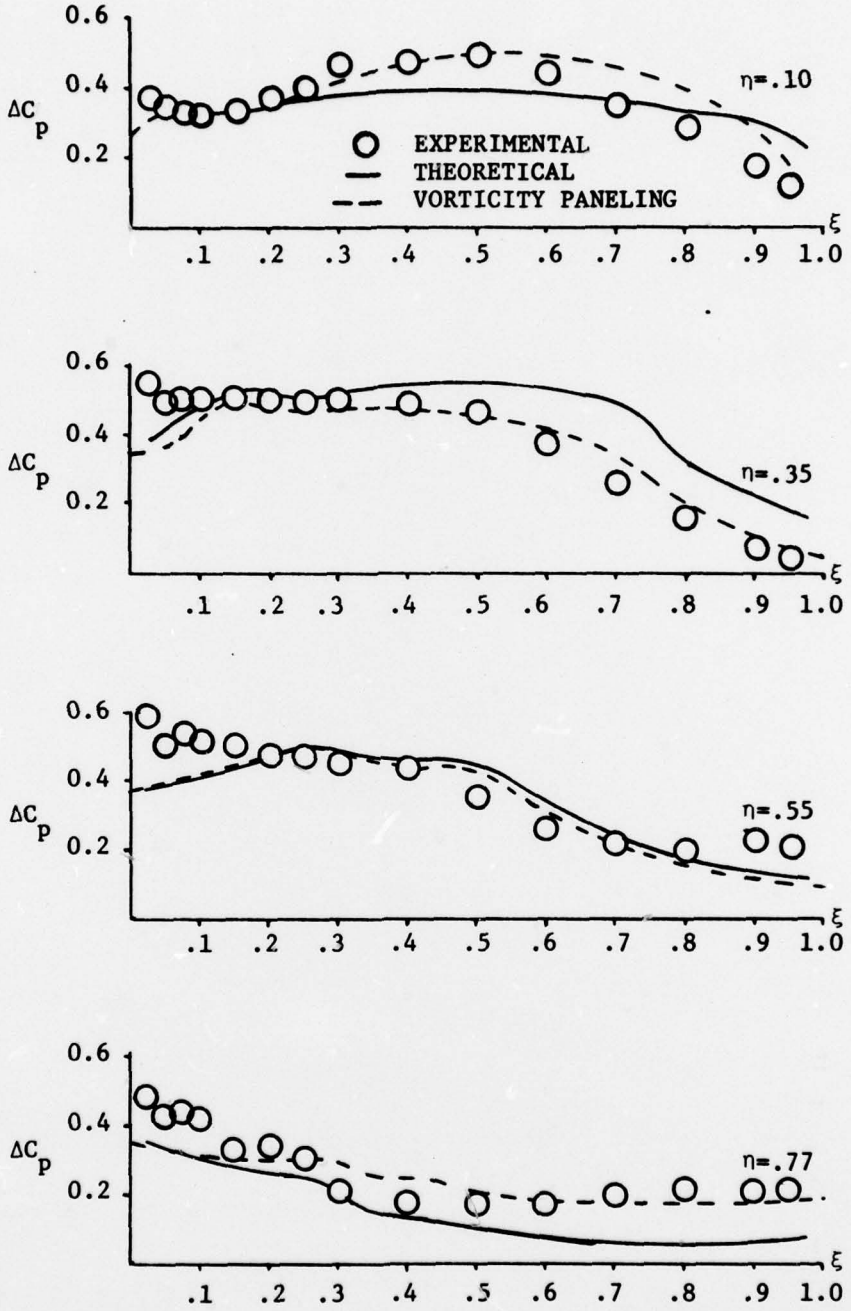

Fig. 15. Pressure Distribution on a Warped Trapezoidal Wing, M=1.61, α=6°.

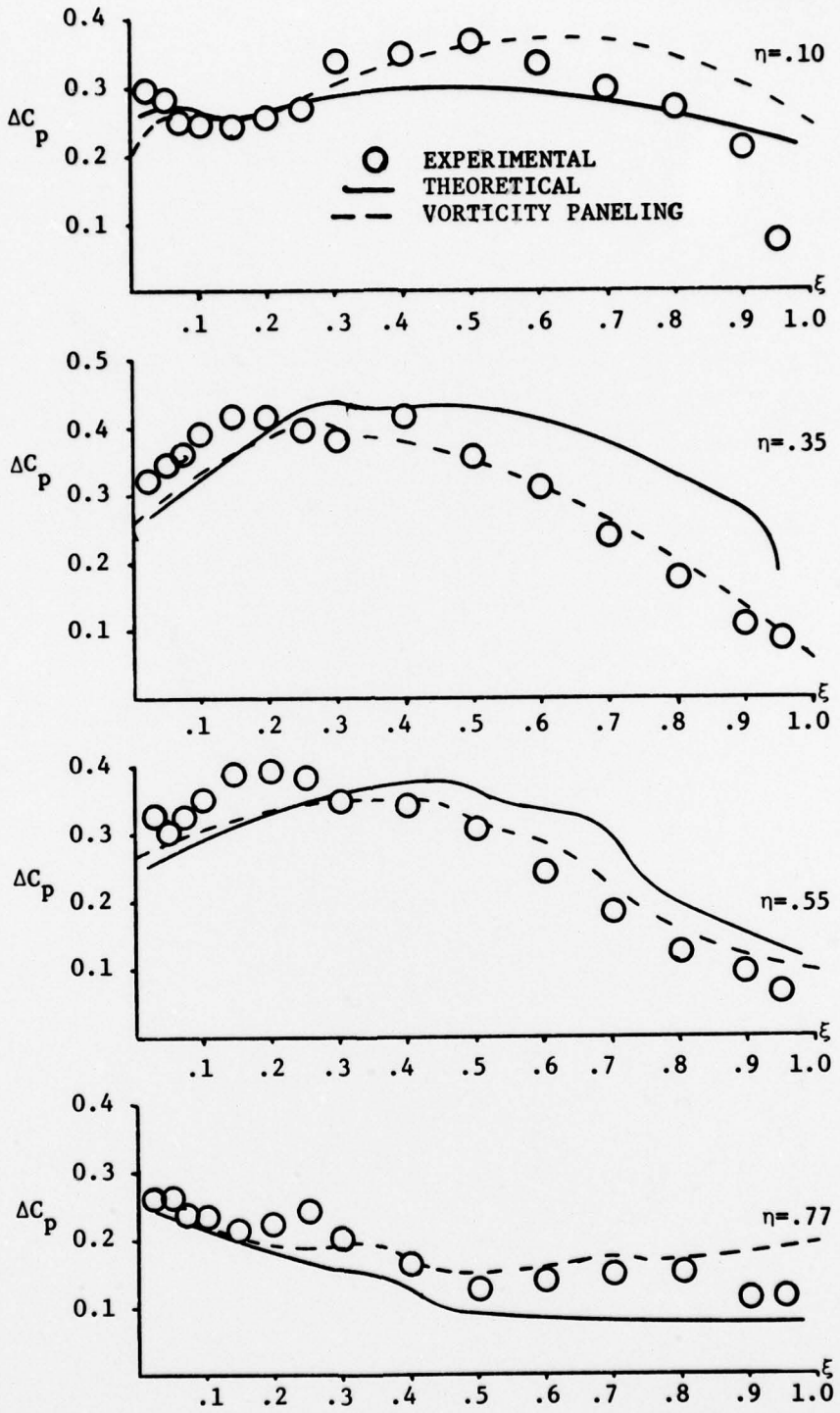

Fig. 16. Pressure Distribution on a Warped Trapezoidal Wing, M=2.01, α=6°.

a wing-body and full span elevon has not as yet been completely analyzed and hence requires additional research.

The missile configuration under study consists of a slender circular body with unwarped, fixed, low aspect ratio, rear mounted, cropped delta wings and constant chord elevons (Fig. 3, wing #2). Since the configuration operates at high Reynolds number, viscosity should not dominate the pressure field so that potential flow theory should be applicable. Since both the wing and elevon are thin, the effects of thickness on the lift are negligible and both may be treated as planar lifting surfaces.

For this particular analysis, body interference effects are accounted for with slender body lift ratios as

$$C_{N_{w(B)}} = C_{N_{\alpha_w}} [K_{w(B)} \alpha_w] \tag{39}$$

where $C_{N_{w(B)}}$ is the normal force on the wing in the presence of the body and $K_{w(B)}$ is the lift ratio factor for the wing-body at angle of attack. The wing is assumed to lie along the body centerline. Lift ratios are based on total loads so only the net effects of the body on the wing or elevon can be determined.

The elevon is located immediately aft of the wing as shown in Fig. 17. The flow just aft of the wing trailing edge is turbulent, as with any blunt trailing edge and impacts on the elevon. The details of the flow field are not well known and are consequently difficult to handle. However, for purposes of this analysis, it was assumed that the wake pressure coefficient is zero such that essentially freestream conditions exist where the wake impacted on the elevon. In short, part of the elevon was

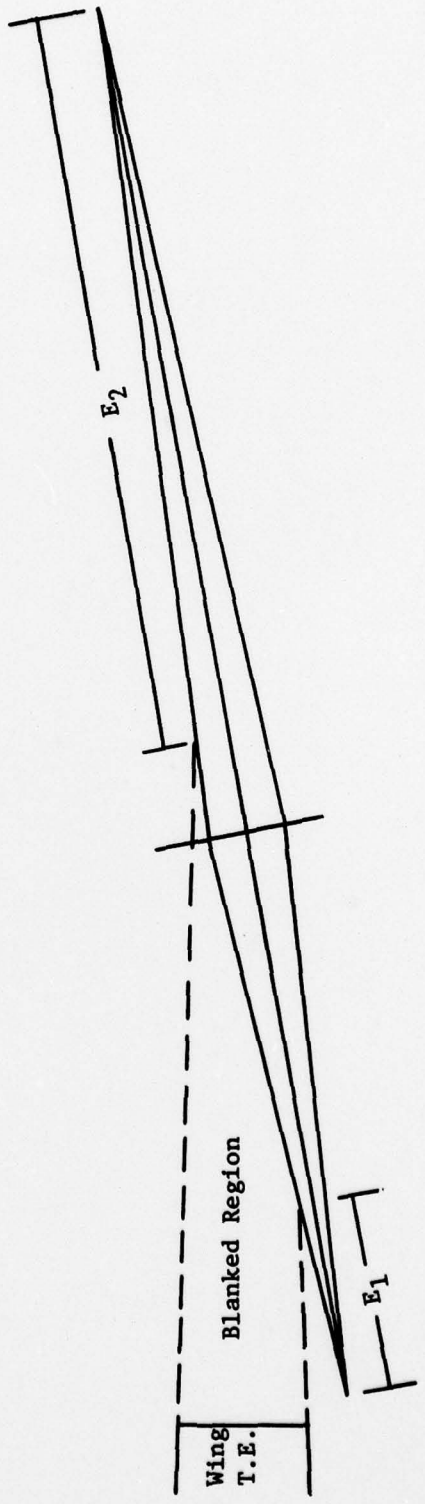

Fig. 17. Sketch of the Elevon-Thick Wing Configuration.

"blanked out" from the rest of the flow field by the wing wake. Thus the elevon was broken up into two separate, smaller lifting surfaces, E_1 and E_2 as depicted on Fig. 17.

The flow was assumed to be tangent to the surface of the aft portion of the wing for all angles of attack. Thus the size and location of the "blanked region" on the elevon was the same for all the no-gap cases.

When the wing is at an angle of attack, the downwash it creates reduces the angle of attack of the flow that the elevon experiences. No wing wake roll-up occurs for this case and thus the wake of the wing downwash was assumed to be flat. Elliptic wing loading and angles of attack were assumed so the normal force and lift were approximately equal.

The downwash angle created by the wing in the presence of the body is given as

$$\varepsilon_w = - \frac{C_{N_{w(B)}}}{\pi \, AR_w} \tag{40}$$

The net elevon angle of attack is then

$$\alpha_E = \alpha_w + \varepsilon_w \, . \tag{41}$$

The angle of attack contributions of the elevon characteristics are distinct from the deflection angle contributions. However, since linear aerodynamics is assumed, the two contributions can be superimposed to determine the overall elevon characteristics.

The strip of the elevon forward of the "blanked region," E_1, also generates downwash as it is assumed to be a separate airfoil. However, calculations indicate the induced angle to be negligibly small in comparison to the elevon deflection angle.

The elevon normal force and hinge moment equations with the thickness effects included, are

$$C_{N_{E(wB)}} = K_{E(B)} C_{N_{\alpha_E}} \alpha_E + k_{E(B)} [C_{N_{\delta_{E_1}}} + C_{N_{\delta_{E_2}}}] \delta_E$$

$$C_{H_{E(wB)}} = K_{E(B)} C_{H_{\alpha_E}} \alpha_E + k_{E(B)} [C_{H_{\delta_{E_1}}} + C_{H_{\delta_{E_2}}}] \delta_E \qquad (42)$$

In terms of the wing angle of attack and downwash angle,

$$C_{N_{E(wB)}} = K_{E(B)} C_{N_{\alpha_E}} (\alpha_w + \varepsilon_w) + k_{E(B)} [C_{N_{\delta_{E_1}}} + C_{N_{\delta_{E_2}}}] \delta_E$$

$$C_{H_{E(wB)}} = K_{E(B)} C_{H_{\alpha_E}} (\alpha_w + \varepsilon_w) + k_{E(B)} [C_{H_{\delta_{E_1}}} + C_{H_{\delta_{E_2}}}] \delta_E \qquad (43)$$

The first comparison of the theory with experimental data is shown in Fig. 18. For this case, both the wing and elevon are modeled as zero thickness flat plates. The analytical results fall below the experimental values but the theory does give the correct trends for normal loading and hinge moment. Figure 19 presents the results for the wing thickness effects. The angle of attack trends are the same as in Fig. 18. Now, however, the analytical results agree with the experimental results much better, particularly the normal force coefficients. Wing thickness, therefore, exerts substantial influence on the elevon aerodynamic characteristics, The discrepancies in magnitude and slope indicate that the very simple flow model used here is not completely accurate.

An investigation of possible wing downwash effects on the size and location of the "blanked region" was made. For this model it was assumed that the induced downwash at the wing trailing edge caused the blanked out region to shift locations on the elevon. The results are presented in

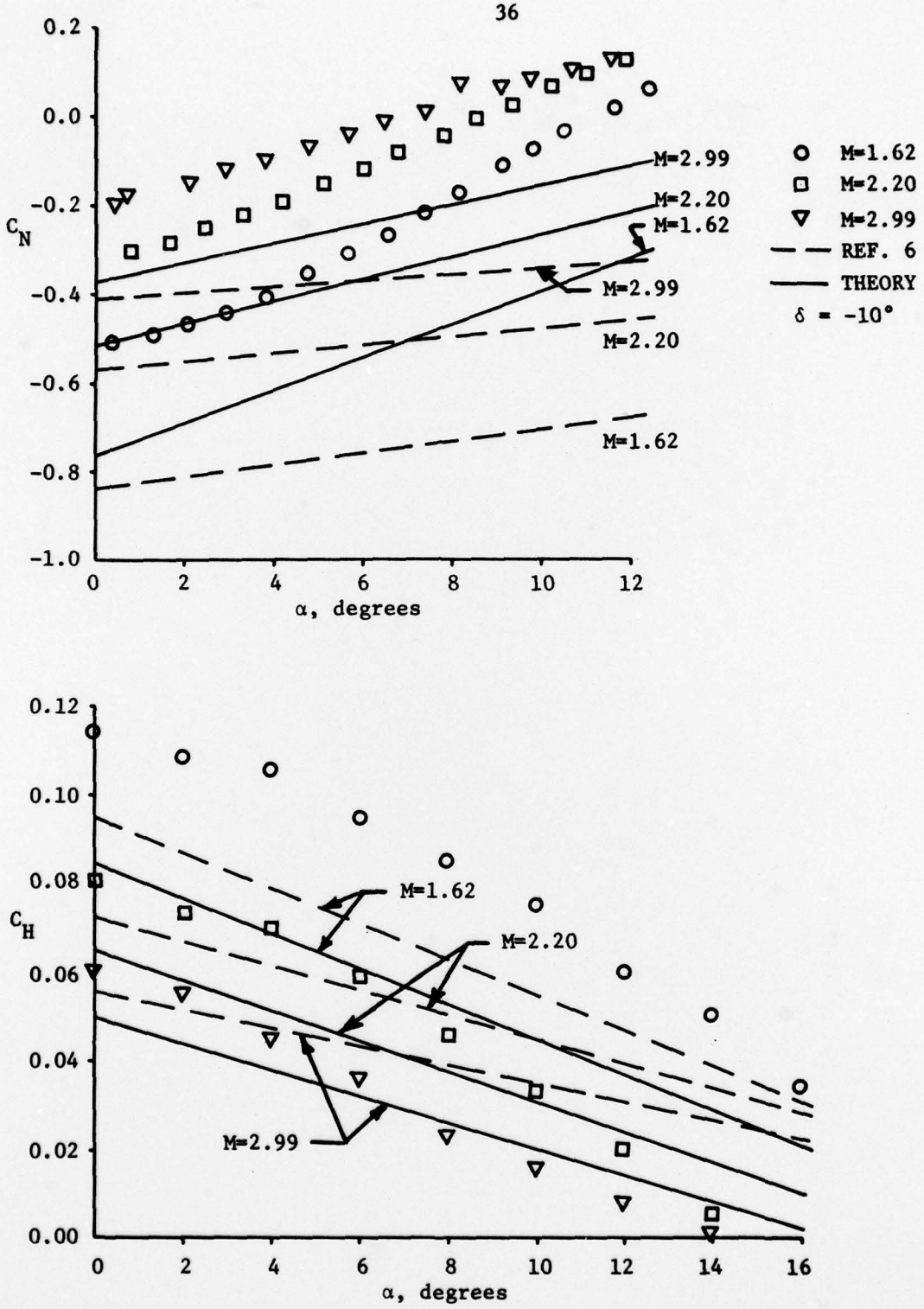

Fig. 18. Normal and Hinge Moment Coefficient for an Elevon in the Wake of a Planar Wing.

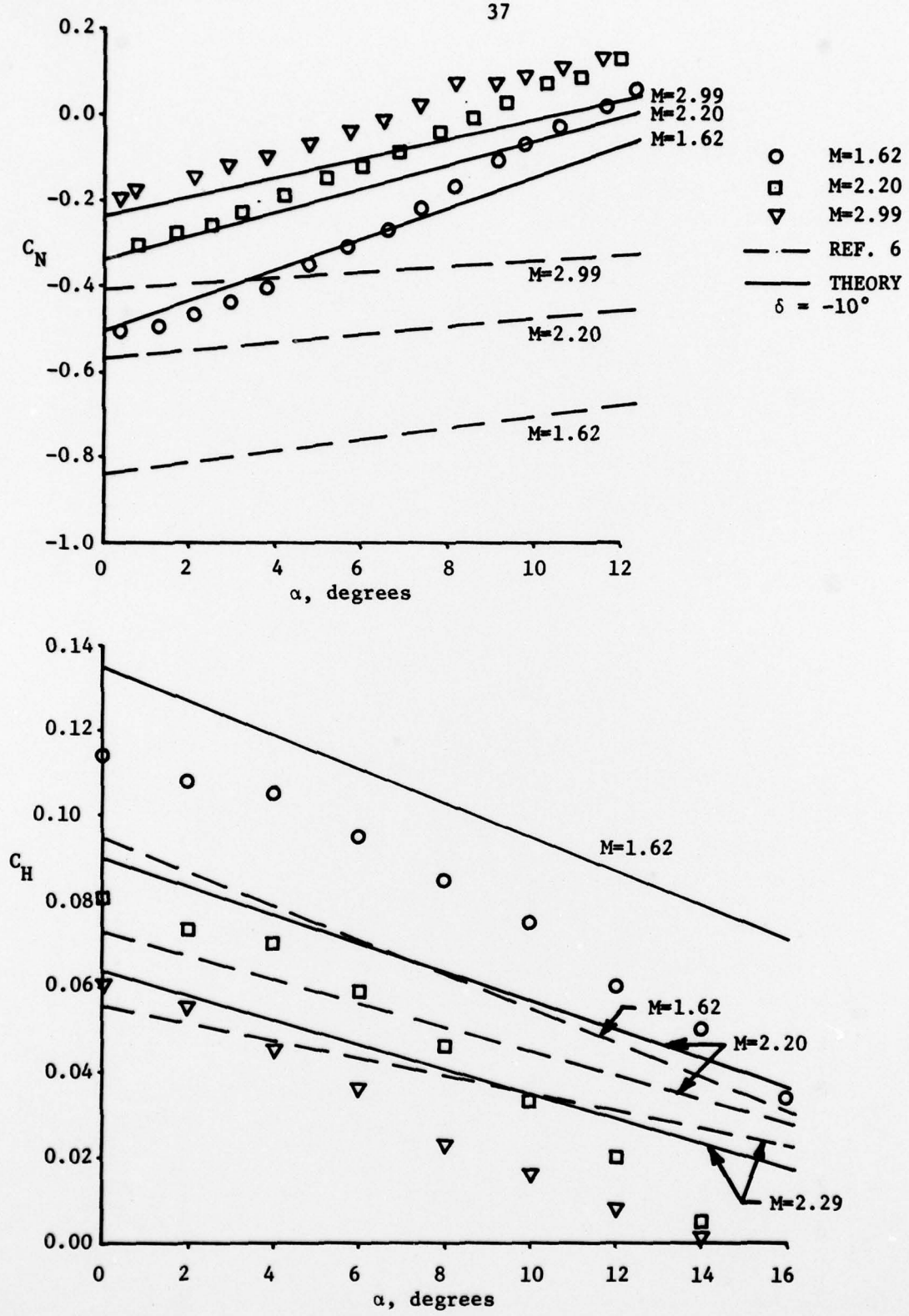

Fig. 19. Normal and Hinge Moment Coefficient for an Elevon in the Wake of a Thick Wing.

Fig. 20. The poor agreement with experimental data indicates that the assumed flow model is not valid and that physically changes in angle of attack, i.e., changes in downwash, do not cause significant alteration in the blanked out region on the elevon.

As a means of reducing the elevon hinge moment, a four-inch cut was made into the trailing edge of the wing so that a gap was formed between the wing and the elevon. In this instance, the elevon was treated as if it were not "blanked out." A comparison with the no-gap configuration is shown in Fig. 21. The theory predicts the experimental results well, if somewhat conservatively. Thus the wing thickness effects are only substantial if the elevon is very close to the wing trailing edge. Additionally, it was observed by Selden[6] that the elevon behaves as if it were in freestream flow when it is deflected -20° or more. Therefore, the wing thickness effects appear to be important only when the elevon is immediately aft of the wing and when it is slightly deflected.

In conclusion, it is quite apparent that wing trailing edge thickness does indeed have significant influence on the loads experienced by the elevon. However, it should be noted that these computations are only preliminary and that a <u>complete</u> model of the flow field has not been established. Further research using numerical techniques (non-potential flow) may be required before the problem is finally solved.

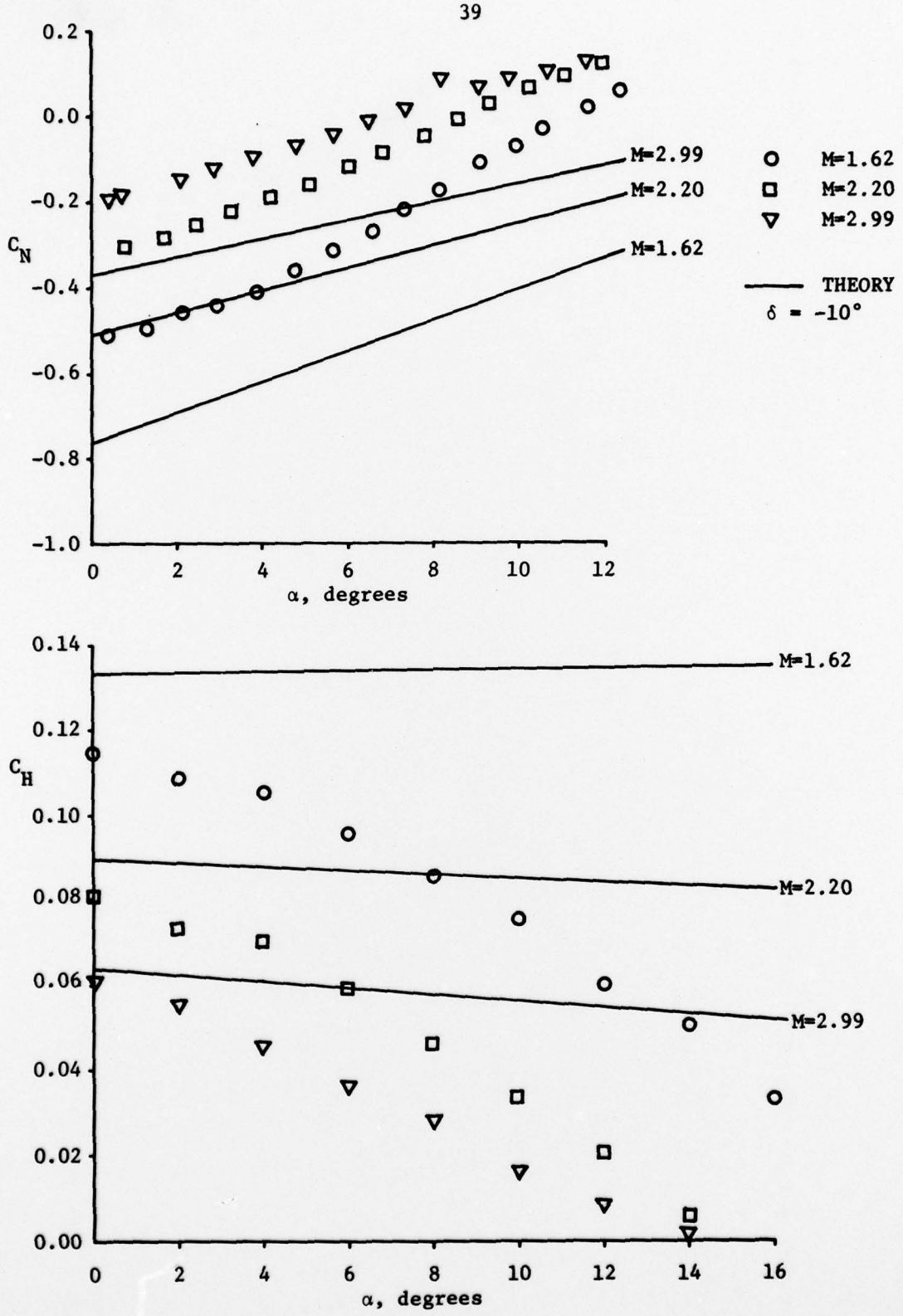

Fig. 20. Normal and Hinge Moment Coefficient for an Elevon in the Wake of a Thick Wing-Downwash Effects.

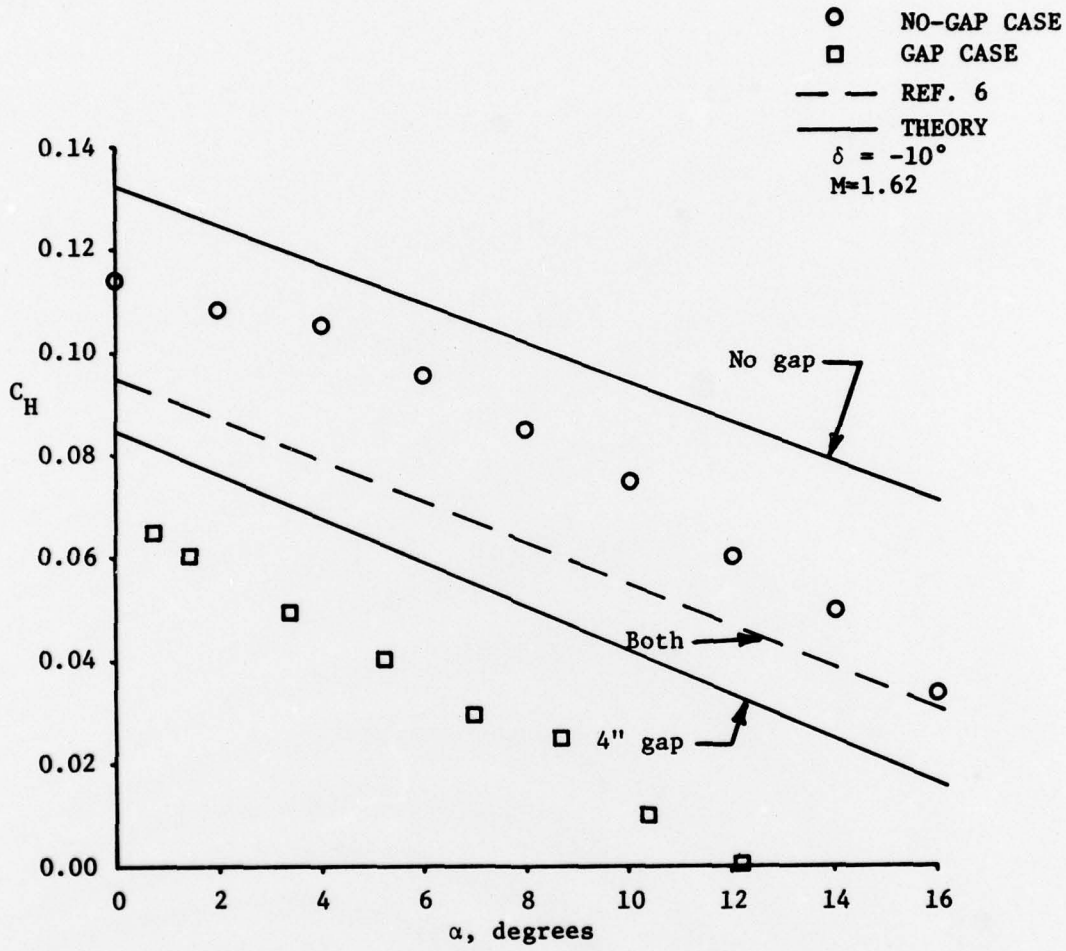

Fig. 21. Hinge Moment Coefficient for an Elevon With and Without a Four-Inch Gap.

IV. REFERENCES

1. Burkhalter, J. E., and Purvis, J. W., "An Aerodynamic Analysis of Deformed Wings in Subsonic and Supersonic Flow," Final Report, Contract No. DAAG29-77-C-0069, U.S. Army Research Office, Research Triangle Park, North Caroline, December 1977.

2. Malvestuto, F. S., Margolis, K., and Ribner, H. S., "Theoretical Lift and Damping in Roll of Thin Sweptback Wings of Arbitrary Taper and Sweep at Supersonic Speeds - Subsonic Leading Edges and Supersonic Trailing Edges," NACA TN 1860, 1949.

3. Harmon, S. M., and Jeffreys, I., "Theoretical Lift and Damping in Roll of Thin Wings with Arbitrary Sweep and Taper at Supersonic Speeds - Supersonic Leading and Trailing Edges," NACA TN 2114, 1950.

4. Landrum, E. J., "A Tabulation of Wind-Tunnel Pressure Data and Section Aerodynamic Characteristics at Mach Numbers of 1.61 and 2.01 for Two Trapezoidal and Three Delta Wings Having Different Surface Shapes," NASA TN D-1394, 1962.

5. Landrum, E. J., "A Tabulation of Wind-Tunnel Pressure Data and Section Aerodynamic Characteristics at Mach Numbers of 1.61 and 2.01 for a Reflex Cambered Wing and a Cambered and Twisted Wing Having the Same Swept Planform," NASA TN D-1393, 1962.

6. Selden, B. S., Goodwin, F. K., and Nielsen, J. N., "Analytical Investigation of Hinge Moments on Missile Trailing-Edge Control Surfaces," Final Report, U.S. Army Missile Command, September 1974.